Immunosuppression broadens evolutionary pathways to treatment failure during *Acinetobacter baumannii* pneumonia

Wenwen Huo[1,§], Lindsay M. Busch [1,2,§], Efrat Hamami[1], Juan Hernandez-Bird[1], Christopher W. Marshall[3,4], Edward Geisinger[5], Vaughn S. Cooper[3], Tim van Opijnen[6], Jason W. Rosch[7] and Ralph R. Isberg[1,*]

[1]Department of Molecular Biology and Microbiology, Tufts University School of Medicine, 150 Harrison Ave., Boston, MA 02111, USA.

[2]Current address: Division of Infectious Diseases, Emory University School of Medicine

[3]Department of Microbiology and Molecular Genetics and Center for Evolutionary Biology and Medicine, University of Pittsburgh School of Medicine, Pittsburgh, Pennsylvania, USA.

[4]Current Address: Dept. of Biological Sciences, Marquette University, 1428 W. Clybourn St., Milwaukee, WI. 53233.

[5]Department of Biology, Northeastern University, Boston, MA, 02115, USA

[6]Department of Biology, Boston College, Boston, MA, USA.

[7]Department of Infectious Diseases, St Jude Children's Research Hospital, Memphis, TN, USA.

[§]Equal contributions.
[*]Corresponding Author

Abstract

Acinetobacter baumannii is increasingly refractory to antibiotic treatment in healthcare settings. As is true of most human pathogens, the genetic path to antimicrobial resistance (AMR) and the role that the immune system plays in modulating AMR during disease are poorly understood. Here we reproduced several routes to fluoroquinolone resistance, performing evolution experiments using sequential lung infections in mice that are replete or depleted of neutrophils, providing two key insights into the evolution of drug resistance. First, neutropenic hosts were demonstrated to act as reservoirs for the accumulation of drug resistance. Selection for variants with altered drug sensitivity profiles arose readily in the absence of neutrophils, while immunocompetent animals restricted the appearance of these variants. Secondly, antibiotic treatment failure was shown to occur without clinically defined resistance, an unexpected result that provides a model for how antibiotic failure occurs clinically in the absence of AMR. The genetic mechanism underlying both these results is initiated by mutations activating the drug egress pump regulator AdeL, which drives persistence in the presence of the antibiotic. Therefore, antibiotic persistence mutations are demonstrated to present a two-pronged risk during disease, causing drug treatment failure in the immunocompromised host while simultaneously increasing the likelihood of high-level AMR acquisition.

Introduction

Acinetobacter baumannii is an emerging Gram-negative pathogen, one of the high-priority ESKAPE organisms that is increasingly refractory to multiple antibiotic treatment regimens[1]. A significant proportion of healthcare-associated diseases that are associated with this group of pathogens, such as ventilator associated pneumonia, is linked to their documented multi-drug resistance (MDR) [2-5]. Of particular importance are patients in intensive care units (ICU) who are critically ill and have depressed immunological clearance mechanisms that increase the risk of infection by MDR pathogens [6,7]. As a consequence, the healthcare environment with its immunologically compromised patients could provide a unique niche for selection of MDR isolates [8]. Overlaying these issues is the fact that for many patients in healthcare settings, antibiotic treatment failure is common but is often unexplained, as resistant organisms cannot be identified[9].

A. baumannii clinical isolates have demonstrated a remarkable ability to successfully battle antibiotic treatment in the clinic, resulting from high intrinsic resistance to antimicrobials and the acquisition of drug resistance elements by the organism.[10,11,12, 13] A critical missing link is a detailed roadmap for the stepwise evolution of antibiotic resistance in the clinic, particularly in identifying *A. baumannii* subpopulations most likely to give rise to drug treatment failure. Furthermore, whether a patient group exists that provides the reservoir for antimicrobial resistance (AMR) acquisition is largely unknown. Particularly for healthcare-associated diseases, patient groups susceptible to *A. baumannii* are by their nature compromised in a number of fashions, with the potential for providing reservoirs for AMR evolution. The range of individuals with altered immune function in these settings may allow for a diversity of host targets that can act as primary amplifiers of resistance, with eventual spread to individuals with different sets of

susceptibilities. Therefore, as a model for healthcare-associated pneumonia we aimed to explore how depletion of a single arm of innate immunity in the mouses often seen in hospitalized patients, could help shape the antibiotic treatment outcome and support evolution of resistant organisms that can spread to others in healthcare settings.

Fluoroquinolones (FQ) such as ciprofloxacin initially showed excellent activity against *A. baumannii* infections[14]. Members of this drug class inhibit bacterial cell growth by covalently linking to DNA gyrase (*gyrA*) and topoisomerase IV (*parC*), leading to double stranded DNA breaks and cell death[15]. Drug resistant mutants arise fairly frequently in the clinic, with over 80% of clinical isolates of *A. baumannii* currently being FQ resistant[16]. The most commonly reported mechanisms of ciprofloxacin resistance in the clinic are target protein alterations and the overexpression of efflux pumps. In *A. baumannii*, alterations in target proteins usually evolve in a stepwise fashion, starting with *gyrA* (usually Ser81Leu) followed by *parC* (Ser83Leu). Interestingly, in addition to the patient's underlying condition and hospitalization status, prior exposure to fluoroquinolone is also a risk factor for *A. baumannii* colonization and infection[17], indicating that resistance to this antibiotic class is linked to either the pathogenic potential of the isolate or is highly associated with acquisition of MDR. Unknown is whether there exist early adaptive mutations that enable precursor populations of *A. baumannii* to act as ancestors to drug resistance.

Given the poor understanding of how antibiotic resistance evolves in the clinic, and the lack of a detailed interrogation of the role played by the immune response in controlling selection of AMR, we sought to identify the steps that lead to resistance in the presence or absence of a single arm of innate immunity. The rationale behind this approach is that clinical antibiotic resistance is associated with mutations located outside well-characterized drug targets,

and these are difficult to identify bioinformatically or predict based on culture studies [18-20]. This approach provides evidence that absence of neutrophil function allows outgrowth of drug persisters and the appearance of fluoroquinolone resistance. In so doing, we tie drug resistance evolution to the problem of unexplained antibiotic treatment failure.

Results

Recapitulation of *Acinetobacter baumannii* evolved drug resistance during pneumonic disease. We serially passaged *A. baumannii* 15 times within a mouse pneumonia model to analyze the dynamics and genetic trajectories of resistance to the FQ antibiotic ciprofloxacin (CIP), with the purpose of determining whether neutrophils play a role in suppressing drug resistance (Fig. 1A). The CIP^S ATCC reference strain 17978 (AB17978) was passaged by oropharyngeal inoculation in either immunocompetent animals or those depleted of neutrophils by pretreatment with two doses of cyclophosphamide. Mice in three parallel lines were CIP treated at 7- and 19- hours post infection (hpi) and bacteria were collected from the lungs of animals euthanized at 27 hpi. The enriched bacterial pools from each independent infection were used as inocula for the next round of infection under the two immune status conditions. The dynamics of bacterial yield was assessed from lung homogenates, and the CIP minimum inhibitory concentration (MIC) of each population was determined followed by whole genome sequencing of the heterogenous pool (mean genome coverage depth: 368.4).

Persistent neutropenia during successive passages quickly results in antibiotic treatment failure. The most striking immediate result from the passage experiments is that the protocol allowed drug resistant mutants to overgrow during passage in neutrophil-depleted animals, while such variants still represented a small population in immunocompetent animals.

After each mouse passage in the presence of CIP, the efficiency of bacterial colonization of the lungs was monitored by quantifying total bacterial colony forming units in the absence of drug (CFU). Bacterial lung yields increased by 1000-fold in CIP-treated neutrophil-depleted mice over the course of 15 passages, as compared to a 10-fold increase in immunocompetent mice (Fig. 1B). After each passage, we observed 10-fold higher colonization in the neutrophil-depleted compared to immunocompetent mice. By passages 5-7, the lung bacterial load in the neutrophil-depleted mice reached the size of the initial inoculum (10^8 CFU), and animals showed significant signs of disease such as lacrimation, piloerection, and decreased mobility in spite of being CIP treated. To determine levels of CIP resistance after each passage, the harvested bacteria were quantified on solid medium in the absence or presence of increasing amounts of drug, plotting the fraction of surviving CFU as a function of CIP concentration (Material and Methods; Fig. 2A and 2C). While there were differences among the three immunocompetent lineages, clinically resistant bacteria (CIP ≥2ug/ml) only started to arise after the 10th passage, with the fraction of these isolates generally comprising less than 1% of the population after 15 passages. Therefore, in immunocompetent mice, 15 passages were insufficient to allow outgrowth and fixation of a resistant population.

The evolutionary trajectories through neutrophil-depleted mice contrasted strongly with immunocompetent mice, as the whole population became CIP resistant over the course of 15 passages. Bacteria resistant to at least 2 μg/ml CIP were observed as early as the 3rd passage (Fig. 2C). After the 9th passage, approximately $1x10^{-5}$ of the bacteria isolated from the neutrophil-depleted mice showed resistance to 8 μg/mL CIP, four times higher than the clinically-defined resistance breakpoint. By 15 passages, almost all bacteria from the neutrophil-depleted lineages were clinically defined as CIP resistant (at concentration of at least 2 μg/mL), with a large

fraction showing resistance to CIP =8 μg/ml. Therefore, resistance acquisition during disease is amplified in the absence of neutrophils.

Clinical failure results from a bacterial population that is clinically defined as drug sensitive. By the 6th passage in neutrophil-depleted mice, yields of bacteria began to approach those observed in the absence of antibiotic (Fig. 1B). Yields remained high in successive passages (Fig. 2C). Therefore, the population that caused drug treatment failure at passage 6 was dominated by bacteria that showed low viability at 2μg/ml, the clinical breakpoint, while more resistant isolates arose from this population during subsequent passages.

To link specific mutational changes over time to these observed phenotypes, we sequenced the pools of genomic DNA isolated from the original inoculum, the parent AB17978 strain, and the pools harvested after the 3rd, 6th, 9th, 12th and 15th passages. Mutation frequencies were then plotted for each passage in the two immune conditions (Fig. 2B and 2D). Based on the predicted sensitivity from the depth of pooled whole genome sequencing, we expected that only nucleotide changes in greater than 5% of the population could be detected (Materials and Methods).

The results from the pooled genomic sequencing allowed us to identify changes associated with either the development of drug resistance, or the lack thereof, in these populations. As predicted from Fig. 2A and the sensitivity limits of the analysis, there was no evidence for mutations driving drug resistance at greater than 5% abundance in the three populations evolved in immunocompetent mice. The only significant alteration, a mutation in a gene encoding a putative solanesyl diphosphate synthase (ACX60_03850; *ispB*) was unrelated to resistance, as single colony isolates showed no increased survival in the presence of CIP (Fig. 2E). It was clear, however, that drug resistance variants were present at low levels in these

populations and rose to about 0.1% by the 15th passage. Two of six randomly selected colonies from the 15th passage that formed colonies on 2μg/ml had the canonical S81L mutation in GyrA. The rest of the strains isolated on CIP plates harbored a combination of four mutations that were similarly found in the neutrophil-depleted lineages, which were subjected to further analysis (Fig. 2E).

Consistent with the dynamic nature of resistance acquisition within the neutrophil-depleted lineages (Fig. 2B), analysis of the population identified the cause of drug treatment failure and uncovered the mutations that drove the stepwise trajectory to CIP^R (Fig. 2D). In all three lineages, a first step mutation occurred within *adeL* between passages 3 and 6 in neutrophil-depleted mice in all three lines. The initial *adeL* mutations were different in each line and disrupted the 3' end of the gene. Previously, mutations in this region of the gene have been shown to activate the AdeFGH pump regulated by AdeL [21,22], and our data are consistent with this interpretation (below, Fig. 3C). Mutations in various other locations arose as second step mutations between passage 9 and 12. For instance, double mutants appeared to overgrow Lineages 1 and 2, while a quadruple mutant appeared to overgrow Lineage 3.

To identify the various genotypes linked with increased CIP resistance, we isolated single colonies after 15 passages with or without CIP (1μg/mL) selection and sequenced two individual purified clones per condition. Indeed, among all single colonies harvested from the neutrophil-depleted lineages, the majority of individual clones accumulated more than one mutation (Fig. 2E). In two lineages of the neutrophil-depleted mouse infections, alleles of DNA gyrase observed infrequently in the clinic, were identified after 15 passages (*gyrA*(A117E) and *gyrB*(Q447H), respectively). Having *gyrA*(A117E) alone was able to raise the CIP MIC by 16-fold (Fig 2E). Clones having the *gyrB*(Q447H) allele were only observed linked to *adeL*(C312*),

resulting in CIP MIC that was 8-fold higher than that of the parent strain (Fig 2E). Besides the mutations in target proteins, other single colonies that resulted in a similar MIC increase were found to have a combination of four mutations (Fig. 2E). When comparing the single colonies isolated that had a CIP of 1 μg/mL to those isolated without antibiotic, the colonies presented the same genomic changes, indicating that the mutants described here became predominant without requiring CIP selection *ex vivo*.

Mutations in *adeL* allow for persistence in the presence of high levels of ciprofloxacin. To deconvolute the function of the various mutations observed, we backcrossed mutations into the parent strain and assessed their relative contributions to CIP resistance. Of particular interest were nucleotide changes identified in populations after the 6th passage in neutrophil-depleted mouse lines, as CIP failed to efficiently restrict growth in the lung in these passages, and this failure was associated with the outgrowth of single *adeL* mutations (Figs. 1A, 2D). The *adeL* gene (ACX60_06025)[22] has two predicted domains often associated with LysR type transcriptional regulators: a helix-turn-helix domain and a substrate binding domain that are responsible for regulation of the AdeEFG pump (Fig. 3A). Of the *adeL* mutations that arose during the *in vivo* passages, one is located within the predicted substrate binding domain while the others are at the C terminal end comprising in-frame deletions or early termination codons (Fig. 3A and 3B). We constructed strains with each of these mutations and observed 100-1000X increased *adeG* transcription levels compared to the parental strain, consistent with AdeFGH efflux pump overproduction (Fig. 3C).

While these single *adeL* mutations resulted in an increase in MIC to ~1 μg/mL CIP (Fig. 4C), this level was below the recognized clinical breakpoint[23] and such strains would be indicated as susceptible. As these are first step mutations, we hypothesize that variants harboring

these changes may facilitate the outgrowth of more resistant isolates by promoting tolerance or persistence in the presence of antibiotic. To test this model, we evaluated the survival of *adeL* mutants during exposure to high levels of CIP [24-28]. Exposure to 10 μg/mL CIP, roughly 20X MIC of the parental strain, led to the majority of the *adeL* mutants (> 99%; MDK99) being rapidly killed (within 1 hour), mimicking what was observed for the parental strain (Fig. 3D). However, unlike the parental strain, a subpopulation was able to persist through 24 hours of drug exposure (Fig. 3D). This phenotype was dependent on pump overproduction, as an *adeL* mutant strain deleted for the *adeFGH* operon was indistinguishable from the parental strain (Fig. 3D). These data argue that *adeL* mutations drive persistence in the presence of CIP *via* increased expression of *adeFGH*, providing a reservoir for the outgrowth of strains with increased resistance.

Resistance of evolved mutants in neutrophil-depleted mice can be explained by combining *adeL* with *mfsA* mutations. We continued backcross analysis to identify the minimal determinants necessary to confer clinical resistance during passage in the mouse. Many of the single colony isolates from lineage 3 at passage 15 of the immunocompromised mice possessed a combination of mutations in four genomic locations: *adeL*, *acfR*, *lpxD*, and the intergenic *rpmL-mfsA* region, the latter of which is located between a ribosomal protein gene and a predicted coding region for a putative MFS transporter (ACX60_15150, annotated as *nreB*; Fig. 2D and 2E). To determine the role in drug susceptibility of each of these mutations, we constructed separate strains carrying single mutations. All single mutants showed various MICs well below 2 μg/ml CIP, with each of the *adeL* mutations as well as *mfsA*(-9) showing increased MICs above the parental strain (Table S1; Fig. 4C). The *mfsA*(-9) mutation is located 9 bp upstream of *mfsA*, within 2 bases of a previously reported mutation selected during evolution of

CIP resistance in *A. baumannii* in planktonic conditions[29]. Consistent with MFS transporter over-production, we found that the *mfsA*(-9) mutation increased the *mfsA* mRNA levels by ~9-fold relative to the parental strain, based on q-rtPCR analysis (Fig. 4B). Significantly, when the *mfsA*(-9) mutation was combined with the *adeL*P131H mutation, the CIP MIC increased to ~4ug/ml and became indistinguishable from the quadruple mutant strain isolated from *in vivo* passage 15 (Fig. 4C; Table S1). Therefore, combining two mutations that resulted in upregulation of both the AdeFGH pump and a putative MFS transporter was sufficient to reconstruct CIP resistance.

A hotspot for mutations within *lpxD* is tightly linked to fluoroquinolone resistance in clinical isolates. The mutation *lpxD* T118_A119insA (locus tag: ACX60_07955; GenBank: AKQ26661.1) was consistently found in CIP^R isolates from mice. This alteration within an acyltransferase involved in lipooligosaccharide (LOS) biosynthesis [30-32] showed no effect on MIC (Table S1)**.** To test for clinical linkage of *lpxD* mutations to drug resistance, we analyzed the genomes of 4671 clinical isolates [33] and identified fluoroquinolone resistant strains based on the *gyrA*S81L resistance allele. The LpxD sequences were identified among this group, and linkage to *gyrA*S81L was tested by plotting z-scores as a function of residue number (Fig. 5B; Material and Methods). Of the CIP resistant isolates, 2762/4062 had alterations at residue E117 (z-score: 8.98; p-value, < 0.00001), which is adjacent to the T118 allele identified in our mouse experiments, with both the E117K and T118_A119insA variants predicted to be in a turn between two beta sheets (Fig. 5C)[34]. Although the significance of this linkage is unclear, the fact that the *lpxD* T118_A119insA has a fitness defect in broth (Fig. 5D), raises the possibility that it could contribute to a persistence phenomenon in tissues leading to evolution of drug resistance.

Evolutionary replay experiments reconstruct the pathway to drug resistance. The observation that a resistant organism outcompeted a persistent strain (Fig. 2D) could be due to a coincidence that occurred during serial passage or due to antibiotic-driven selection for strains with increased MIC over persistent strains. To distinguish between these possibilities for the neutrophil-depleted Lineage 3 variants, we performed two evolutionary replay experiments [35]. In the first (Fig. 6A, B), bacteria were harvested after passage 9 and cycled 3 times in duplicate in neutrophil-depleted animals to test if the *adeL* I335A336 allele would again be outcompeted by initially rare drug-resistant mutants (Fig. 2D). The second approach was to mix a colony-purified drug persistent *adeL* I335A336 single mutant (P9Cy3.1; Table S1) with a colony-purified drug resistant quadruple mutant (Cy31; Table S1) in the approximate ratio present at passage 9 (95:5), before passaging three times (Material and Methods; Fig. 6C).

In both experiments, we observed an increase in bacterial burden and fraction of bacteria showing CIP MIC >2 after passaging the pools in neutrophil-depleted CIP-treated mice (Supp. Fig. 1). Whole genome sequencing of the bacterial populations harvested after each passage revealed a near identical evolutionary trajectory as seen from the original experiment, with the single mutant associated with drug persistence eventually outcompeted by drug resistant mutants (Fig. 6). Remarkably, in one of our replicate lineages (Fig. 6A), a new mutation arose in the intergenic region between *rpmL* and *mfsA* (*mfsA*(-19)), arguing for the contribution of this regulatory region in resistance evolution. Analyzed in isolation from other mutations, strains harboring *mfsA*(-19) behaved similarly to single mutants having the previously described *mfsA*(-9) mutation, as it results in a similar increase in MIC values (Fig. 4C), and is associated with up-regulation of *mfsA* transcript levels (Fig. 4B). Therefore, this demonstrates that the evolutionary

trajectory is reproducible, and can be regenerated by phenotypically similar mutations that arise spontaneously.

Ciprofloxacin treatment within the host simultaneously selects for increased resistance and enhanced fitness. Antibiotic resistance is often associated with a fitness cost[36] that may be compensated over time by continued selection on secondary genotypes that overcome these costs. As a consequence, mutants with high resistance could maintain their selective advantage over non or low-resistance mutants even in the absence of drug treatment. To test this model, the relative fitness of the drug resistant mutants derived from neutrophil-depleted lineages was compared to the parent strain AB17978. In the absence of CIP, variants isolated after passage in neutrophil-depleted mice showed varying degrees of subtle growth impairment in broth relative to the parental strain (Fig. 7A; Cy11, $p < 0.02$). Similar results were observed when the mutants were challenged in competition with the WT strain in immunocompetent animals, although the differences did not consistently rise to the level of statistical significance. (Fig. 7B).

The lowered fitness of mutants, however, did not directly test the model that selection in neutropenic mice increased fitness relative to first-step CIP^R variants. In the absence of CIP treatment, the parent strain outcompeted the Lineage 3 quadruple mutant isolate Cy31 (Table S1) under neutrophil-depleted conditions, similar to results observed in the presence of immune function (Fig. 7C; Cy31 against WT). Nonetheless, the Cy31 strain had a clear fitness advantage over its predecessor Lineage 3 *adeL* mutant when competed in the absence of antibiotics (Fig. 7C; Cy31 against P9Cy3.1). Therefore, in competition with the persister mutant, ciprofloxacin simultaneously selected for an isolate with increased CIP resistance and enhanced fitness relative to mutant competitors in the absence of drug. This predicts that drug-resistant mutants are able to

evolve to heightened relative fitness and replace persister mutants. As fitness increases, resistant mutants should be able to compete with sensitive strains even after cessation of antibiotic treatment, potentially escalating treatment failure and providing fertile ground for the emergence of resistant strains with high fitness even in immunocompetent hosts.

Discussion

Comparative analyses of bacterial pathogen databases indicate that clinical antibiotic resistance is associated with mutations located outside well-characterized drug targets [18-20]. Analysis of clinical resistance is often retrospective, with a few exceptional studies that have allowed identification of a timeline of bacterial resistance in human populations[24-28,37-39]. Our study bridges an important gap in understanding how resistance evolves, by following experimental evolution of fluoroquinolone resistance in a pneumonia disease model. Strikingly, in the absence of one arm of immune pressure, *A. baumannii* resistance arose after few passages in murine lungs during CIP treatment (Fig. 1B), resulting in treatment failure. Conversely, while there was a small subpopulation having clinically-defined resistance to CIP in healthy immunocompetent mice, the overall frequency remained low and this did not lead to treatment failure (Fig. 1B) (Fig. 2A).

Importantly, the spectrum of selected mutations was altered by the absence of neutrophils. In contrast to the canonical target site *gyrA*S81L mutation observed in immunocompetent animals, the *gyrA*A117E and *gyrB*Q447H alleles rarely observed in clinical strains predominated in two of the lines from neutrophil-depleted animals (Fig 2E; 6 out of 12 CIP resistant clones). These unusual isolates showed clear fitness defects during disease and in culture (Fig. 6). These non-canonical *gyrA* and *gyrB* mutations with low fitness may be unlikely to arise in the presence of intact immune functions, which is consistent with evolutionary trajectories being determined by the immunological state of the host. Therefore, we propose that immunocompromised hosts are incubators for the generation of unique drug resistant variants, with uncertain outcomes after pathogen exposure to the community at large. Although the variants we described have reduced fitness relative to WT, continued passage demonstrated that

stepwise increase in drug resistance was associated with stepwise increase in fitness (Fig. 7). Similar fitness effects have been obtained during continued passage in culture[29]. The recent demonstration of enhanced viral evolution of SARS-CoV-2 in an immunocompromised patient undergoing therapeutic antibody treatment is a graphic example of the potential interplay between immunity, antimicrobials and evolution in the clinic, with potential largescale community effects [40]. In fact, persistence mutants have been demonstrated to arise during continued antibiotic therapy in an immunocompromised patient treated for vancomycin-resistant enterococcus[41], further tying the results presented here with documented clinical outcomes.

Antibiotics primarily act by targeting essential cellular functions or pathways [42,43]. In response to transient antibiotic exposure, a proportion of bacteria typically persist or tolerate this treatment with mutations arising that can increase the fraction of the surviving population[44-46]. The mechanisms for allowing persistence/tolerance likely differ between bacterial species and vary among antibiotics[47], but it is generally agreed that persistence/tolerance is caused by cell dormancy[48-50] or transient expression of efflux pumps and stress response pathways[24,51]. Furthermore, persistence/tolerance mechanisms may play an important role in the relapse of bacterial infections [52-54]. In our study, we found that persistence in *A. baumannii* can be promoted by upregulation of a drug efflux pump, AdeFGH [22]. It is known that many clinical isolates are found to overproduce efflux pumps that remove multiple antibiotics from the bacterial cytoplasm[22,55], and that antibiotic persistence is associated with such pump upregulation[56,57]. Therefore, it is likely that this is a common motif for initiating the evolutionary path to drug resistance. Of particular note, mutations upregulating this pump are rarely isolated in the laboratory through simple antibiotic single-step selections on solid agar, indicating there may be a special environment in the lung that allows outgrowth of these mutants.

There are three important repercussions from the analysis of the AdeL efflux overproducer mutations. First, overproduction results in drug treatment failure during pneumonic disease in the mouse, in spite of the fact that these bacterial strains are CIP-sensitive based on the international standard for clinical breakpoints[23]. Therefore, clinical drug treatment failure in the absence of identified antibiotic resistance[9] could be explained by the outgrowth of drug persistent mutants, taking advantage of fluctuations in drug availability to the infection site between doses. Second, the mutation provides a molecular basis for *A. baumannii* to develop second-step variants that lead to CIP resistance above the clinical breakpoint. Of interest, inhibitors of efflux pumps have been suggested to re-sensitize bacteria to multiple antibiotics[58], but perhaps such a regimen may also delay progression to resistance. Finally, isolates from drug treatment failure occurring in immunocompromised patients could generate a pool of precursor mutants giving rise to resistant isolates that eventually infect a broad range of patients.

We here propose a model of bacterial resistance progression in immunodepleted hosts (Fig. 8). When infecting a host, the antibiotic susceptible bacteria colonize at a relatively low rate. With active transmission and continuous CIP treatment, bacterial persisters arise that have MICs below the clinical breakpoint, increasing bacterial load at the infection site. On continued treatment, or transfer to a similar host undergoing CIP treatment, fully resistant mutants outgrow the population. Although the presence of intact immune function may delay outgrowth of such mutants, the fact that we could identify a mutant with a persister allele in the presence of immune function indicates that such alleles could act as enablers of drug resistance in all hosts.

Genomic analyses can identify allelic variants linked to drug resistance, but verifying the functional importance of these alleles is hindered by founder effects that are often difficult to discount. The *lpxD* E117K mutation is one such allele associated with resistant *gyrA* S81L-

containing genomes. The fact that during multiple passages in immune-depleted mice the adjacent *lpxD* T118 insA allele was isolated argues for a role of these altered residues in supporting the outgrowth of drug resistant organisms. The *lpxD* T118 insA mutation likely has an effect on envelope function. This raises the possibility that the mutation causes subtle changes in permeability that slow drug access to target, or else the slowed growth of strains harboring this allele increases drug tolerance during growth in tissues[47]. Our inability to demonstrate increased tolerance to CIP and the fact that the clinical *lpxD* E117K did not show a fitness defect when grown in LB broth (Fig. 5D) argues that the critical phenotypes may be observed exclusively during growth in tissues, making them difficult to evaluate.

In summary, we hypothesize that resistance progression in clinical isolates follows a similar trend witnessed in our experiments, albeit perhaps with greater complexity in the human. Drug sensitive bacteria may colonize both healthy and immune system-compromised patients, but resistance evolution occurs more rapidly within hosts having impaired neutrophil function. The canonical resistance mutations that arise within healthy individuals may compete efficiently with host-evolved mutations in patients having impaired neutrophil function. Hence, the transmission from individuals having intact immune function may pose risks to immunocompromised patients. Adding to the risks subjected to vulnerable patients, we found that *A. baumannii* persistence mutants with MIC levels below the clinical breakpoint were associated with treatment failure, emphasizing the difficulty in treating these patients (Fig. 1B) [9,59-62]. While heterogeneity and variability between infected patients is inevitable, this work provides insight into some genetic factors that could predispose individuals to treatment failures in specific clinical contexts. Future work should be focused on how this evolutionary trend

towards drug resistance can be controlled, such as tackling the molecular basis for selection of persister or other mutations that lead to treatment failure.

Material and Methods

Bacterial Strains. Bacterial strains used in this study are listed in Table S1. *Acinetobacter baumannii* strains are derivatives of ATCC 17978. Bacteria were grown in Lysogeny Broth (LB) (10 g/L tryptone, 5 g/L yeast extract, 10 g/L NaCl) or on LB agar plates (LB supplemented with 15g/L agarose). Broth cultures were grown at 37°C in flasks with orbital shaking at 200 rpm or in tubes with rotation on a roller drum at 56 rpm. Growth was monitored by measuring absorbance spectrophotometrically at 600 nm (A_{600nm}). Plates were incubated at 37°C. Antibiotics were used at the following concentrations: Gentamicin: 10 μg/mL (*A. baumannii*) and 50 μg/mL (*E. coli*); Carbenicillin: 100 μg/mL.

Murine experimental evolution. The *in vivo* passaging experiments were performed identically in either immunocompetent or neutrophil-depleted 6-8 weeks-old female BALB/C mice (Fig. 1A). Neutrophil depletion was induced via cyclophosphamide pretreatment [63]. Briefly, 150 mg/kg and 100 mg/kg of cyclophosphamide monohydrate (Sigma-Aldrich: C7397) were administered 4 days and 1 day prior to infection, respectively. At the time of infection, mice were transiently anesthetized by inhalation of isoflurane and lung infections were established using ~10^8 colony forming units (CFU) of *A. baumannii* from mid-log phase cultures (A_{600nm} ~0.5) via the oropharyngeal aspiration [64]. At 7 and 19 hours post infection (hpi), 100 mg/kg of ciprofloxacin (Sigma-Aldrich: PHR1044) was administered via subcutaneous injection. At 27 hpi, mice were euthanized, and lungs were removed aseptically and homogenized in 1 mL of ice-cold 1x phosphate buffered saline (PBS). Afterwards, the homogenate was plated on large (150 x 15 mm) LB agar plates and incubated for ~17 hours at 37°C. The total number of bacteria was quantified using CFU. The enriched bacteria were scraped off the LB plates and resuspended in

1x PBS. The resuspension was used for DNA isolation as well as the inoculum for the next passage/round of infection (stored at -80°C in 20% glycerol prior to use). For each round of mouse infection/passage, bacterial frozen stocks were revived by diluting them in LB broth and growing them to exponential phase. Afterwards, ~10^8 CFU of the pool was used to establish infection in each mouse. Three separate lineages of murine infections were maintained in parallel in each condition (immunocompetent or neutrophil depleted), and within each lineage each starting inoculum was passaged 15 times. Validation experiments involving the reconstruction of identified mutants and re-passaging of these strains in mice were similarly performed with the only difference being that the infection was terminated at 24 hpi instead of at 27 hpi.

Determining the fraction of resistance to set ciprofloxacin concentrations in each pool. To evaluate the fraction of bacteria acquired from each passage that are viable on culturing in various concentration of ciprofloxacin, the glycerol stock of each pool was revived in fresh LB broth and grown to exponential phase. A total of ~10^7 CFU were used for serial dilutions in 1x PBS and 10 μl from each diluted culture was spotted on LB agar plates containing the following concentrations of ciprofloxacin: 0, 0.25, 0.5, 1, 2, 4 and 8 μg/ml. After an overnight incubation at 37°C, colonies were counted, and CFU/ml was calculated. A detection limit of 100 CFU/ml was used. The fraction bacteria resistant to a certain concentration (C_0; $C_0 > 0$) of ciprofloxacin is calculated as (CFU/ml at C_0 - CFU/ml at all concentrations above C_0) / Total CFU. A stacked bar plot of the data was generated using Prism GraphPad (Fig. 2).

Whole Genome Sequencing. Genomic DNA (gDNA) was extracted from bacteria using the DNeasy Blood and Tissue kit (Qiagen). Library preparation was performed using Illumina

Nextera with previously described modifications [65]. Libraries were enriched with 8 cycles of PCR and sequenced using HiSeq2500 at Tufts University Core Facility using single-end 100 bp reads. Reads were aligned to the *A. baumannii* ATCC 17978 genome and its plasmids (GenBank Accession: CP012004; pAB1: CP000522; pAB2: CP00523; pAB3: CP012005), and variants were identified at 5% cutoff using breseq 0.32 [66]. The predicted functional impact of substitution variants was determined by using PROVEAN [67].

Competition Assays. Competition experiments were performed as described previously[64]. Briefly, designated strains were grown to exponential phase (A_{600nm} ~ 0.5-1.0) and mixed at a 1:1 ratio for the inoculum. Afterwards, ~10^8 CFU of the bacterial mixture was used to challenge WT or cyclophosphamide-treated BALB/C mice via the oropharyngeal route as described for the mouse passage experiments. 24 hr post inoculation, lungs were removed aseptically, homogenized and extracts were spread on LB agar plates. To quantify the input and output ratio of each designated strain, both the inoculum and the lung homogenate were serially diluted in 1x PBS and plated on LB agar as well as LB agar supplemented with 2 μg/mL of ciprofloxacin to differentiate between the WT and CIP resistant test strains. Competitive index (CI) was calculated as CI = output (unmarked/marked) / input (unmarked/marked).

Persistence Assay. *A. baumannii* was grown in 3 individual LB broth cultures overnight from separate colonies. The cultures were diluted 1000-fold into 8 ml LB broth and incubated by rotation at 37°C for 2-3 hours until reaching mid or late exponential growth (A_{600nm} ~ 0.3-0.8). Ciprofloxacin was added to reach a final concentration of 10 μg/ml, the concentration regarded as 20x the MIC for the parent ATCC 17978 *A. baumannii* strain. These cultures were then

incubated at 37ºC for up to 24 hours. After 0, 1, 3, 6, and 24 hours, 500 µl of culture was removed, washed twice in 1x PBS, resuspended in 500 µl PBS, and sequentially diluted in 1x PBS. Serial dilutions were used for CFU quantification by spot plating on LB agar plates. Dilution factors harboring quantities ranging from 3-35 CFUs were used to calculate the CFU/mL. The limit of detection by this assay was determined to be 375 CFUs. The CFU/mL across the biological replicates at each time point throughout the drug challenge were plotted as mean ± Standard Error of Mean.

qRT-PCR gene expression analysis. Bacteria were grown to early stationary phase in LB broth, RNA was harvested and purified using RNeasy kit (Qiagen) followed by cDNA synthesis using SuperScript VILO cDNA kit (Thermo Fisher). The cDNA was then amplified with PowerUp SYBR Green Master Mix (Applied Biosystems) via a StepOnePlus Real-Time PCR system (Applied Biosystems) per manufacturer's instructions, and target amplification efficiency was evaluated by generating a standard curve with dilutions of cDNA (>95% amplification efficiency for each primer pair). Primers were designed to amplify regions of around 150 bp internal to genes (Table S1). Triple technical replicates were examined per biological sample and at least three biological replicates per strain were tested, with controls lacking reverse-transcriptase included to verify a lack of contaminant genomic DNA. Transcript levels of specific targets from each strain were evaluated by the comparative $2^{-\Delta\Delta Ct}$ method to the parental strain, normalizing to that of the endogenous control 16s. The transcript level for each target across biological replicates was plotted as mean ± Standard Error of Mean (Fig. 3&4).

MIC determination. Minimum inhibitory concentrations (MICs) were determined by broth microdilution. Overnight cultures of strains of interest were diluted 1000X in fresh LB broth and grown to mid-logarithmic phase (A_{600} ~0.5). Afterwards, cultures were diluted to a final A_{600} = 0.003 and tested in the presence of two-fold dilutions of antibiotics. 200 μl of culture-antibiotic mixture was then aliquoted to a 96 well plate (COSTAR) and technical duplicates were performed in a Biotek plate reader with rotation. Growth was monitored by measuring A_{600} at 15 min. intervals for 16 hr, and the MIC was determined as the lowest concentration of drug that prevented growth, using at least three biological replicates for each strain. The MICs across biological replicates were plotted as mean ± Standard Error of Mean (Fig. 4).

Molecular cloning and mutant construction. Plasmids and primers used in this study are listed in Table S1. The mutant strains were constructed through sequential cloning into pUC18[68] then pJB4648[69] as previously described[13]. Briefly, the mutant allele from each strain of interest was amplified alongside upstream and downstream segments to generate a PCR product ~1500 bp in length flanked by appropriate restriction sites. The PCR product was then ligated into pUC18 and propagated in *E. coli* DH5α. The PCR product was then subcloned from pUC18 into pJB4648 and propagated in *E. coli* DH5α λpir. After sequence confirmation, the pJB4648 plasmid construct containing the desired mutation was introduced into *A. baumannii* via electroporation. Markerless, in-frame mutations were isolated via homologous recombination as described [13].

Comparative sequence analysis. The LpxD protein sequence from ATCC 17978 was compared to genomes downloaded from PATRIC database using tblastn to identify the amino acid location of mismatches and gaps. In total, 4671 genomes were split into three groups: those with a GyrA S81L mutation; those with the same GyrA sequence as in AB17978; and the rest. Within each group, the mismatches/gaps at each amino acid location within LpxD were displayed as number of genomes having mismatches/gaps at that location. A table of the data was constructed showing the specific amino acid in the rows, the genome groups harboring these mutations in the columns, and the total number of mismatches/gaps in the cells. The results in each cell were then normalized using *z*-scores with the mean and standard deviation from individual genome groups. The *z*-score was plotted as function of each residue.

Calculation of doubling time in broth culture. Overnight cultures of bacteria were diluted 1000-fold in fresh LB broth and grown for 8 hours. The A_{600} values were measured every hour using a spectrophotometer, and the log2 transformed values were plotted as a function of time (hr). To calculate the doubling time, a modified sigmoid function ($y = \frac{L1}{e^{-k(x-x0)}+1} - L2$) was fitted to the plotted curve(y: log2 transformed A_{600} value, x: time in hrs, x_0: timepoint when the growth rate was the fastest, k, L1, L2: rate constants), with the fastest growth rate for each culture determined as the time in which second derivative of the fitted curve approached 0 (or when $x = x0$), at which point the doubling time was represented as the inverse of the slope ($\Delta t = {}^{4}/_{k * L1}$) (Code available at: https://github.com/huoww07/calulate_bacteria_doubling_time). To evaluate the goodness-of-fit, the R^2 value was calculated for each growth curve assay (the R^2 ranges from 0 to 1, representing the worst to the best fit). At least three biological replicates were

performed for each test strain (Table S2, Table S3) and the average doubling time and standard deviation was calculated. Significance was determined using Student two-tailed t-test.

Accession numbers.

The datasets generated during the current study are available in the Sequence Read Archive (PRJNA485355).

Acknowledgements

This work is supported by NIAID U01AI12430 to TvO, JWR, VSC and RI, NIH R21AI128328 to RI and T32AI07422 support for JH-B. We thank the colleagues in all of our labs for support and constant critiquing of the experimental strategies used here.

Author Contributions

RI, JR and TvO devised the study. LB and JH performed the mice experiments. WH, EH and JH performed the wet-lab experiments. WH and LB performed the whole genome sequencing and bioinformatics analyses. CM, VC, EG and TvO collaborated on the bioinformatics analyses and performed training. WH, LM, EH, JH and RI interpreted the results and wrote the manuscript. WH, LB, EH, JH, CM, EG, VC, TvO, JR and RI approved the final manuscript.

Figure legends

Figure 1. Continuous passaging of *A. baumannii* in a lung infection model results in early antibiotic failure in neutrophil-depleted mice. A). The 15-passage strategy using the pneumonia model in both immunocompetent and neutrophil-depleted mice. Neutrophil depletion was induced by two doses of cyclophosphamide at 72- and 24-hrs prior of infection. At the time of infection, *A. baumannii* ATCC 17978 was oropharyngeally inoculated into mice at 10^8 CFU, and two doses of CIP were administered at 9- and 19-hrs post infection. At 27-hrs post infection, the mice were euthanized, lungs were homogenized, and bacteria were plated on LB agar plates . After overnight growth, the bacteria were collected and 10^8 CFU used for the next round of infection/passage. B). Rapid development of antibiotic failure as a consequence of passage in the absence of neutrophils. After lungs were homogenized, total CFU on LB agar in the absence of antibiotic were determined and plotted as function of passage number. Shown are three lines (L1, L2, L3) for immunocompetent and neutrophil-depleted animals treated with CIP as described in panel (A).

Figure 2. High level ciprofloxacin resistance evolves in a stepwise fashion during passage in neutrophil-depleted mice. (A,C). After each passage, bacteria from lung homogenates were serially diluted onto LB agar containing noted concentrations of CIP (μg/ml). The fraction of CFU on the graded series of CIP plates was determined for each pool and displayed in stacked bar plots for immunocompetent (A) and neutrophil-depleted (C) mouse infection lineages. The limit of detection was 2.7E-6. (B,D) The gDNA from each bacterial pool was isolated and subject to whole genome sequencing to identify the genomic mutations acquired throughout passaging (after passage 3, 6, 9, 12 and 15). The mutations were detected using a 5% abundance

cutoff and filtered against the parent strain AB17978. The relative abundance of each mutation was plotted as a function of passage number from (B) immunocompetent lineages and (D) neutrophil-depleted lineages (D). (E) After 15 passages, the bacterial pool from each lineage was grown on LB with or without CIP (1 μg/mL) to select for single colonies. Colonies were purified and subject to whole genome sequencing and MIC assays. In (E), each column represents a single colony and the rows represent selection criteria, individual mutations and MIC values. The detected mutations with >90% frequency were aggregated for all colonies and the presence of each mutation in a certain colony was highlighted in purple. MICs were labeled and color-coded for all colonies.

Figure 3. *adeL* mutations drive bacterial persistence through over-expression of the AdeFGH pump. (A). Sites of nonsynonymous changes during *in vivo* passaging and domain structure of AdeL. (B). Locations of nonsynonymous changes on predicted functional domains of AdeL. (C). Mutations in *adeL* selected during mouse passage result in specific overproduction of an AdeL-regulated gene *adeG*. Data were determined by qRT-PCR analysis of pump-encoding components *adeG* (regulated by AdeL) or *adeB* and *adeJ* (components of other pumps) in noted *adeL* mutant backgrounds. (D). Overproduction of AdeL-regulated pump components results in increased persistence in presence of CIP. AB17978 derivatives described in legend were exposed to CIP at 20X MIC for noted times and titered for viability by quantitating CFUs.

Figure 4. The presence of mutations in *adeL* and *mfsA* is sufficient to explain CIP^{R} in strains derived from mouse passage experiments. A) Two mutations located directly upstream of *mfsA* selected during mouse passaging experiments. B) Transcription levels of *mfsA* and *rpmL*

were determined by qRT-PCR in strains harboring the two mutations upstream of *mfsA*. ****, p < 0.0001. C) Double mutants containing *adeL* and *mfsA* mutations show MICs of CIP that are indistinguishable from evolvedquadruple mutant strain. Data are mean MICs ± SEM.

Figure 5. The LpxD E117K allele is tightly linked to clinical fluoroquinolone resistance. Assembled genomes of 4671 clinical isolates were obtained from PATRIC database[33]. A). Fraction of genomes having the *gyrA*S81L resistance allele. Among the downloaded genomes, 4062 genomes presented the GyrA S81L allele (shown in red), 386 genomes had the same GyrA allele as ATCC 17978 (shown in green) and the rest had other alleles (shown in black). B) LpxD sequences from all genomes were aligned and compared to ATCC 17978 and the total number of variants per defined amino acid was calculated for each group of genomes. The total number of amino acid changes were normalized and presented as z-scores for each of the three groups, plotted against the residue numbers. C). Structure of *Chlamydia trachomatis* LpxD protein [34] showing the presumed site of the *A. baumannii* E117 based on sequence similarity. D). Broth growth of AB17978 strains differing by single changes in *lpxD*. Shown are strains harboring either the WT, *lpxD* T118A119_insA or *lpxD* E117K alleles.

Figure 6. The evolutionary trajectories of isolates acquired throughout passaging in neutrophil-depleted mice is due to fitness advantage in presence of drug. (A,B) A single *adeL* mutant is outcompeted during infection of CIP-treated mice by a quadruple mutant having drug resistant *adeLmfsA* alleles. The passage 9 pool was oropharyngeally inoculated into neutrophil-depleted mice in duplicate and passaged three times, subjecting each passage to deep sequencing. Displayed are relative abundance of all mutations identified in deep sequencing

pools of the duplicate (panels A,B) passaging experiments as a function of the passage number. C) Competition of purfied *adeL* and quadruple mutant having *adeLmfsA* alleles in presence of CIP results in predominance of the quadruple mutant. The two strains were mixed at a ratio 95:5 (single:quadruple mutant), and oropharyngeally inoculated into neutrophil-depleted mice in the presence of CIP through three successive passages. Deep sequencing of the initial inoculum and each subsequent passage was performed to determine the ratio of the two strains, and the relative abundance of each mutation is displayed as a function of passage.

Figure 7. Simultaneous selection for increased resistance and fitness. A) Growth rates in broth culture of noted isolates from passage in mice. B) Neutrophil-replete and C) Neutrophil depleted (cyclophosphamide treated) BALB/C mice were challenged with noted strain combination to determine relative competition index of each pair of strains. C.I. values were determined by C.I. = (strain1/strain2 output ratio)/(strain1/strain2 input ratio) (Materials and Methods). Data are mean $\pm$ SEM, with significance determine by one-way ANOVA followed by Multiple Comparison. *$p<0.05$; ****$p<0.0001$.

Figure 8. Model of bacterial resistance progression. The antibiotic susceptible inoculum (blue) colonizes poorly in presence of antibiotic. During continued passage with CIP, in the absence of neutrophils, the persister mutants (yellow) arise as first step mutations showing intermediate MICs. With continued passage under the same antibiotic treatment regime, second step mutations arise that have increased fitness in the presence of antibiotic (red) and dominate the population.

Supplemental Figure 1. Bacterial load and resistance levels to CIP after re-passaging. A) The bacterial load harvested from the lungs after each passage is plotted against the passage number for each lineage. B) CIP resistance level of each pool (after each passage) was assayed via quantification of CFU on LB agar supplemented with CIP.

Competing Interests Statement

The authors declare that they have no conflict of interest.

Reference

1 Boucher, Helen W. *et al.* Bad Bugs, No Drugs: No ESKAPE! An Update from the Infectious Diseases Society of America. *Clin. Infect. Dis.* **48**, 1-12, doi:10.1086/595011 (2009).

2 Valentine, S. C. *et al.* Phenotypic and Molecular Characterization of *Acinetobacter baumannii* Clinical Isolates from Nosocomial Outbreaks in Los Angeles County, California. *J. Clin. Microbiol.* **46**, 2499-2507, doi:10.1128/jcm.00367-08 (2008).

3 Sievert, D. M. *et al.* Antimicrobial-Resistant Pathogens Associated with Healthcare-Associated Infections Summary of Data Reported to the National Healthcare Safety Network at the Centers for Disease Control and Prevention, 2009–2010. *Infect. Control Hosp. Epidemiol.* **34**, 1-14, doi:10.1086/668770 (2015).

4 Karlowsky, J. A., Hoban, D. J., DeCorby, M. R., Laing, N. M. & Zhanel, G. G. Fluoroquinolone-Resistant Urinary Isolates of *Escherichia coli* from Outpatients Are Frequently Multidrug Resistant: Results from the North American Urinary Tract Infection Collaborative Alliance-Quinolone Resistance Study. *Antimicrob. Agents Chemother.* **50**, 2251-2254, doi:10.1128/aac.00123-06 (2006).

5 Azim, A. *et al.* Epidemiology of bacterial colonization at intensive care unit admission with emphasis on extended-spectrum β-lactamase- and metallo-β-lactamase-producing Gram-negative bacteria – an Indian experience. *J. Med. Microbiol.* **59**, 955-960, doi:10.1099/jmm.0.018085-0 (2010).

6 Montefour, K. *et al. Acinetobacter baumannii*: an emerging multidrug-resistant pathogen in critical care. *Crit. Care Nurse* **28**, 15-25; quiz 26 (2008).

7 Zeighami, H., Valadkhani, F., Shapouri, R., Samadi, E. & Haghi, F. Virulence characteristics of multidrug resistant biofilm forming *Acinetobacter baumannii* isolated from intensive care unit patients. *BMC Infect. Dis.* **19**, doi:10.1186/s12879-019-4272-0 (2019).

8 Dijkshoorn, L., Nemec, A. & Seifert, H. An increasing threat in hospitals: multidrug-resistant *Acinetobacter baumannii*. *Nat. Rev. Microbiol.* **5**, 939-951, doi:10.1038/nrmicro1789 (2007).

9 Ryan, K. *et al.* The impact of initial antibiotic treatment failure: Real-world insights in healthcare-associated or nosocomial pneumonia. *J. Infect.* **77**, 9-17, doi:10.1016/j.jinf.2018.04.002 (2018).

10 Wong, D. *et al.* Clinical and Pathophysiological Overview of *Acinetobacter* Infections: a Century of Challenges. *Clin. Microbiol. Rev.* **30**, 409-447, doi:10.1128/CMR.00058-16 (2017).

11 Fernandez-Cuenca, F. Relationship between beta-lactamase production, outer membrane protein and penicillin-binding protein profiles on the activity of carbapenems against clinical isolates of *Acinetobacter baumannii*. *J. Antimicrob. Chemother.* **51**, 565-574, doi:10.1093/jac/dkg097 (2003).

12 Lolans, K., Rice, T. W., Munoz-Price, L. S. & Quinn, J. P. Multicity outbreak of carbapenem-resistant *Acinetobacter baumannii* isolates producing the carbapenemase OXA-40. *Antimicrob. Agents Chemother.* **50**, 2941-2945, doi:10.1128/AAC.00116-06 (2006).

13 Geisinger, E. & Isberg, R. R. Antibiotic modulation of capsular exopolysaccharide and virulence in *Acinetobacter baumannii*. *PLoS Pathog.* **11**, e1004691, doi:10.1371/journal.ppat.1004691 (2015).

14 Aldred, K. J., Kerns, R. J. & Osheroff, N. Mechanism of quinolone action and resistance. *Biochemistry* **53**, 1565-1574, doi:10.1021/bi5000564 (2014).

15 Redgrave, L. S., Sutton, S. B., Webber, M. A. & Piddock, L. J. V. Fluoroquinolone resistance: mechanisms, impact on bacteria, and role in evolutionary success. *Trends Microbiol.* **22**, 438-445, doi:10.1016/j.tim.2014.04.007 (2014).

16 Hujer, K. M. *et al.* Rapid Determination of Quinolone Resistance in *Acinetobacter spp. J. Clin. Microbiol.* **47**, 1436-1442, doi:10.1128/jcm.02380-08 (2009).

17 Munoz-Price, L. S. & Weinstein, R. A. *Acinetobacter* infection. *N. Engl. J. Med.* **358**, 1271-1281, doi:10.1056/NEJMra070741 (2008).

18 Saroj, S. D., Clemmer, K. M., Bonomo, R. A. & Rather, P. N. Novel Mechanism for Fluoroquinolone Resistance in *Acinetobacter baumannii*. *Antimicrob. Agents Chemother.* **56**, 4955-4957, doi:10.1128/aac.00739-12 (2012).

19 Osińska, A., Harnisz, M. & Korzeniewska, E. Prevalence of plasmid-mediated multidrug resistance determinants in fluoroquinolone-resistant bacteria isolated from sewage and surface water. *Environ. Sci. Pollut. Res.* **23**, 10818-10831, doi:10.1007/s11356-016-6221-4 (2016).

20 Elhosseiny, N. M., Elhezawy, N. B. & Attia, A. S. Comparative proteomics analyses of *Acinetobacter baumannii* strains ATCC 17978 and AB5075 reveal the differential role of type II secretion system secretomes in lung colonization and ciprofloxacin resistance. *Microb. Pathog.* **128**, 20-27, doi:10.1016/j.micpath.2018.12.039 (2019).

21 Yoon, E. J. *et al.* Contribution of resistance-nodulation-cell division efflux systems to antibiotic resistance and biofilm formation in *Acinetobacter baumannii*. *mBio* **6**, doi:10.1128/mBio.00309-15 (2015).

22 Coyne, S., Rosenfeld, N., Lambert, T., Courvalin, P. & Perichon, B. Overexpression of resistance-nodulation-cell division pump AdeFGH confers multidrug resistance in *Acinetobacter baumannii*. *Antimicrob. Agents Chemother.* **54**, 4389-4393, doi:10.1128/AAC.00155-10 (2010).

23 USCAST. The United States Committee on Antimicrobial Susceptibility Testing (USCAST). Breakpoint tables for interpretation of MIC and zone diameterresults. Version 6.0. (2020).

24 Brauner, A., Fridman, O., Gefen, O. & Balaban, N. Q. Distinguishing between resistance, tolerance and persistence to antibiotic treatment. *Nat. Rev. Microbiol.* **14**, 320-330, doi:10.1038/nrmicro.2016.34 (2016).

25 Kussell, E., Kishony, R., Balaban, N. Q. & Leibler, S. Bacterial persistence: a model of survival in changing environments. *Genetics* **169**, 1807-1814, doi:10.1534/genetics.104.035352 (2005).

26 Balaban, N. Q. Persistence: mechanisms for triggering and enhancing phenotypic variability. *Curr. Opin. Genet. Dev.* **21**, 768-775, doi:10.1016/j.gde.2011.10.001 (2011).

27 Balaban, N. Q. *et al.* Definitions and guidelines for research on antibiotic persistence. *Nat. Rev. Microbiol.* **17**, 441-448, doi:10.1038/s41579-019-0196-3 (2019).

28 Liu, J., Gefen, O., Ronin, I., Bar-Meir, M. & Balaban, N. Q. Effect of tolerance on the evolution of antibiotic resistance under drug combinations. *Science* **367**, 200-204, doi:10.1126/science.aay3041 (2020).

29 Santos-Lopez, A., Marshall, C. W., Scribner, M. R., Snyder, D. J. & Cooper, V. S. Evolutionary pathways to antibiotic resistance are dependent upon environmental structure and bacterial lifestyle. *eLife* **8**, doi:10.7554/eLife.47612 (2019).

30 Raetz, C. R. H., Reynolds, C. M., Trent, M. S. & Bishop, R. E. Lipid A Modification Systems in Gram-Negative Bacteria. *Annu. Rev. Biochem.* **76**, 295-329, doi:10.1146/annurev.biochem.76.010307.145803 (2007).

31 Lathe, R. & Lecocq, J. P. The firA gene, a locus involved in the expression of rifampicin resistance in *Escherichia coli*. *Mol. Gen. Genet.* **154**, 53-60, doi:10.1007/bf00265576 (1977).

32 Kelly, T. M., Stachula, S. A., Raetz, C. R. & Anderson, M. S. The firA gene of *Escherichia coli* encodes UDP-3-O-(R-3-hydroxymyristoyl)-glucosamine N-acyltransferase. The third step of endotoxin biosynthesis. *J. Biol. Chem.* **268**, 19866-19874 (1993).

33 Davis, J. J. *et al.* The PATRIC Bioinformatics Resource Center: expanding data and analysis capabilities. *Nucleic Acids Res.* doi:10.1093/nar/gkz943 (2019).

34 Buetow, L., Smith, T. K., Dawson, A., Fyffe, S. & Hunter, W. N. Structure and reactivity of LpxD, the N-acyltransferase of lipid A biosynthesis. *Proc. Nat. Acad. Sci.* **104**, 4321-4326, doi:10.1073/pnas.0606356104 (2007).

35 Blount, Z. D., Lenski, R. E. & Losos, J. B. Contingency and determinism in evolution: Replaying life's tape. *Science* **362**, doi:10.1126/science.aam5979 (2018).

36 Melnyk, A. H., Wong, A. & Kassen, R. The fitness costs of antibiotic resistance mutations. *Evol. Appl.* **8**, 273-283, doi:10.1111/eva.12196 (2014).

37 Subedi, D., Vijay, A. K., Kohli, G. S., Rice, S. A. & Willcox, M. Comparative genomics of clinical strains of *Pseudomonas aeruginosa* strains isolated from different geographic sites. *Sci. Rep.* **8**, doi:10.1038/s41598-018-34020-7 (2018).

38 Lieberman, T. D. *et al.* Genetic variation of a bacterial pathogen within individuals with cystic fibrosis provides a record of selective pressures. *Nat. Genet.* **46**, 82-87, doi:10.1038/ng.2848 (2013).

39 Lieberman, T. D. *et al.* Parallel bacterial evolution within multiple patients identifies candidate pathogenicity genes. *Nat. Genet.* **43**, 1275-1280, doi:10.1038/ng.997 (2011).

40 Choi, B. *et al.* Persistence and Evolution of SARS-CoV-2 in an Immunocompromised Host. *N. Engl. J. Med.* **383**, 2291-2293, doi:10.1056/NEJMc2031364 (2020).

41 Honsa, E. S. *et al.* RelA Mutant Enterococcus faecium with Multiantibiotic Tolerance Arising in an Immunocompromised Host. *mBio* **8**, doi:10.1128/mBio.02124-16 (2017).

42 Ma, C., Yang, X. & Lewis, P. J. Bacterial Transcription as a Target for Antibacterial Drug Development. *Microbiol. Mol. Biol. Rev.* **80**, 139-160, doi:10.1128/mmbr.00055-15 (2016).

43 van Hoek, A. H. A. M. *et al.* Acquired Antibiotic Resistance Genes: An Overview. *Front. Microbiol.* **2**, doi:10.3389/fmicb.2011.00203 (2011).

44 Moyed, H. S. & Bertrand, K. P. hipA, a newly recognized gene of *Escherichia coli* K-12 that affects frequency of persistence after inhibition of murein synthesis. *J. Bacteriol.* **155**, 768-775, doi:10.1128/JB.155.2.768-775.1983 (1983).

45 Schumacher, M. A. *et al.* HipBA-promoter structures reveal the basis of heritable multidrug tolerance. *Nature* **524**, 59-64, doi:10.1038/nature14662 (2015).

46 Pontes, M. H., Groisman, E. A. & Garsin, D. A. A Physiological Basis for Nonheritable Antibiotic Resistance. *mBio* **11**, doi:10.1128/mBio.00817-20 (2020).

47 Trastoy, R. *et al.* Mechanisms of Bacterial Tolerance and Persistence in the Gastrointestinal and Respiratory Environments. *Clin. Microbiol. Rev.* **31**, doi:10.1128/cmr.00023-18 (2018).

48 Balaban, N. Q., Merrin, J., Chait, R., Kowalik, L. & Leibler, S. Bacterial persistence as a phenotypic switch. *Science* **305**, 1622-1625, doi:10.1126/science.1099390 (2004).

49 Lewis, K. Persister cells, dormancy and infectious disease. *Nat. Rev. Microbiol.* **5**, 48-56, doi:10.1038/nrmicro1557 (2007).

50 Shah, D. *et al.* Persisters: a distinct physiological state of *E. coli*. *BMC Microbiol.* **6**, 53, doi:10.1186/1471-2180-6-53 (2006).

51 Nandakumar, M., Nathan, C. & Rhee, K. Y. Isocitrate lyase mediates broad antibiotic tolerance in *Mycobacterium tuberculosis*. *Nat. Commun.* **5**, doi:10.1038/ncomms5306 (2014).

52 Michiels, J. E., Van den Bergh, B., Verstraeten, N. & Michiels, J. Molecular mechanisms and clinical implications of bacterial persistence. *Drug Resist. Updat.* **29**, 76-89, doi:10.1016/j.drup.2016.10.002 (2016).

53 Fisher, R. A., Gollan, B. & Helaine, S. Persistent bacterial infections and persister cells. *Nat. Rev. Microbiol.* **15**, 453-464, doi:10.1038/nrmicro.2017.42 (2017).

54 Van den Bergh, B., Fauvart, M. & Michiels, J. Formation, physiology, ecology, evolution and clinical importance of bacterial persisters. *FEMS Microbiol. Rev.* **41**, 219-251, doi:10.1093/femsre/fux001 (2017).

55 Yoon, E. J., Courvalin, P. & Grillot-Courvalin, C. RND-type efflux pumps in multidrug-resistant clinical isolates of *Acinetobacter baumannii*: major role for AdeABC overexpression and AdeRS mutations. *Antimicrob. Agents Chemother.* **57**, 2989-2995, doi:10.1128/AAC.02556-12 (2013).

56 Pu, Y. *et al.* Enhanced Efflux Activity Facilitates Drug Tolerance in Dormant Bacterial Cells. *Mol. Cell* **62**, 284-294, doi:10.1016/j.molcel.2016.03.035 (2016).

57 Harms, A., Maisonneuve, E. & Gerdes, K. Mechanisms of bacterial persistence during stress and antibiotic exposure. *Science* **354**, doi:10.1126/science.aaf4268 (2016).

58 Frimodt-Møller, J. & Løbner-Olesen, A. Efflux-Pump Upregulation: From Tolerance to High-level Antibiotic Resistance? *Trends Microbiol.* **27**, 291-293, doi:10.1016/j.tim.2019.01.005 (2019).

59 Peeters, P. *et al.* The impact of initial antibiotic treatment failure: real-world insights in patients with complicated, health care-associated intra-abdominal infection. *Infect. Drug Resist.* **12**, 329-343, doi:10.2147/idr.S184116 (2019).

60 Soriano, A., Mensa, J., Meylan, S., Morata, L. & Kuehl, R. When antibiotics fail: a clinical and microbiological perspective on antibiotic tolerance and persistence of *Staphylococcus aureus*. *J. Antimicrob. Chemother.* **75**, 1071-1086, doi:10.1093/jac/dkz559 (2020).

61 Meylan, S., Andrews, I. W. & Collins, J. J. Targeting Antibiotic Tolerance, Pathogen by Pathogen. *Cell* **172**, 1228-1238, doi:10.1016/j.cell.2018.01.037 (2018).

62 Karve, S. *et al.* The impact of initial antibiotic treatment failure: Real-world insights in patients with complicated urinary tract infection. *J. Infect.* **76**, 121-131, doi:10.1016/j.jinf.2017.11.001 (2018).

63 Wang, E. *et al.* Pathogenesis of Pneumococcal Pneumonia in Cyclophosphamide-Induced Leukopenia in Mice. *Infect. Immun.* **70**, 4226-4238, doi:10.1128/iai.70.8.4226-4238.2002 (2002).

64 Nielsen, T. B., Yan, J., Luna, B. & Spellberg, B. Murine Oropharyngeal Aspiration Model of Ventilator-associated and Hospital-acquired Bacterial Pneumonia. *J. Vis. Exp.* doi:10.3791/57672 (2018).

65 Geisinger, E., Mortman, N. J., Vargas-Cuebas, G., Tai, A. K. & Isberg, R. R. A global regulatory system links virulence and antibiotic resistance to envelope homeostasis in *Acinetobacter baumannii*. *PLoS Pathog.* **14**, e1007030, doi:10.1371/journal.ppat.1007030 (2018).

66 Deatherage, D. E. & Barrick, J. E. Identification of mutations in laboratory-evolved microbes from next-generation sequencing data using breseq. *Methods Mol. Biol.* **1151**, 165-188, doi:10.1007/978-1-4939-0554-6_12 (2014).

67 Choi, Y., Sims, G. E., Murphy, S., Miller, J. R. & Chan, A. P. Predicting the functional effect of amino acid substitutions and indels. *PLoS One* **7**, e46688, doi:10.1371/journal.pone.0046688 (2012).

68 Yanisch-Perron, C., Vieira, J. & Messing, J. Improved M13 phage cloning vectors and host strains: nucleotide sequences of the M13mpl8 and pUC19 vectors. *Gene* **33**, 103-119, doi:10.1016/0378-1119(85)90120-9 (1985).

69 Andrews, H. L., Vogel, J. P. & Isberg, R. R. Identification of linked *Legionella pneumophila* genes essential for intracellular growth and evasion of the endocytic pathway. *Infect. Immun.* **66**, 950-958, doi:10.1128/IAI.66.3.950-958.1998 (1998).

70 Hanahan, D., Jessee, J. & Bloom, F. R. Plasmid transformation of *Escherichia coli* and other bacteria. *Methods Enzymol.* **204**, 63-113, doi:10.1016/0076-6879(91)04006-a (1991).

71 Kolter, R., Inuzuka, M. & Helinski, D. R. Trans-complementation-dependent replication of a low molecular weight origin fragment from plasmid R6K. *Cell* **15**, 1199-1208, doi:10.1016/0092-8674(78)90046-6 (1978).

72 Bouvet, P. J. M. & Grimont, P. A. D. Taxonomy of the Genus *Acinetobacter* with the Recognition of *Acinetobacter baumannii sp. nov., Acinetobacter haemolyticus sp. nov., Acinetobacter johnsonii sp. nov.*, and *Acinetobacter junii sp. nov*. and Emended Descriptions of *Acinetobacter calcoaceticus* and *Acinetobacter lwoffii*. *Int. J. Syst. Bacteriol.* **36**, 228-240, doi:10.1099/00207713-36-2-228 (1986).

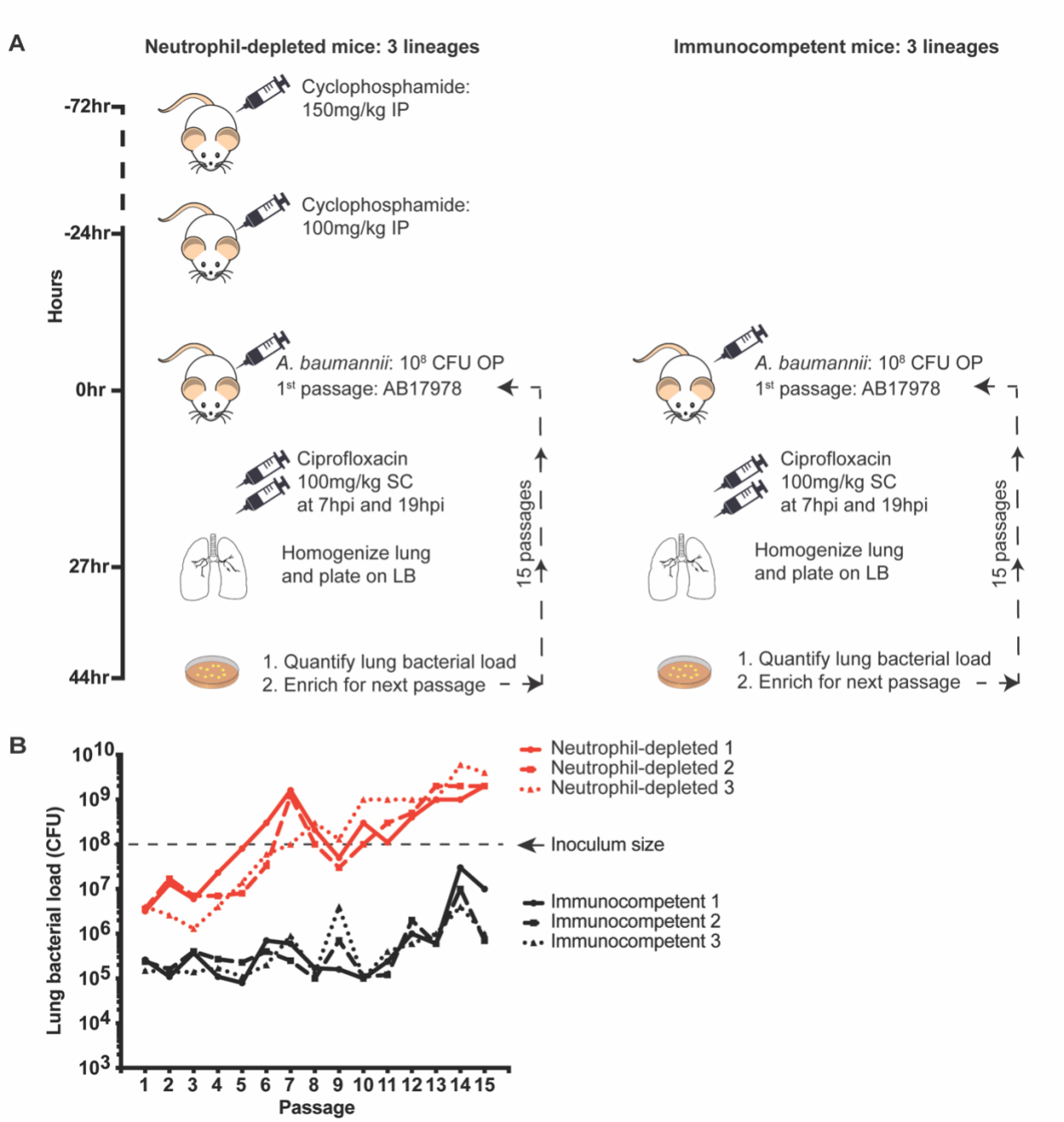

Figure 1. Continuous passaging of *A. baumannii* in a lung infection model results in early antibiotic failure in neutrophil-depleted mice. A). The 15-passage strategy using the pneumonia model in both immunocompetent and neutrophil-depleted mice. Neutrophil depletion was induced by two doses of cyclophosphamide at 72- and 24-hrs prior of infection. At the time of infection, *A. baumannii* ATCC 17978 was oropharyngeally inoculated into mice at 10^8 CFU,

and two doses of CIP were administered at 9- and 19-hrs post infection. At 27-hrs post infection, the mice were euthanized, lungs were homogenized, and bacteria were plated on LB agar plates . After overnight growth, the bacteria were collected and 10^8 CFU used for the next round of infection/passage. B). Rapid development of antibiotic failure as a consequence of passage in the absence of neutrophils. After lungs were homogenized, total CFU on LB agar in the absence of antibiotic were determined and plotted as function of passage number. Shown are three lines (L1, L2, L3) for immunocompetent and neutrophil-depleted animals treated with CIP as described in panel (A).

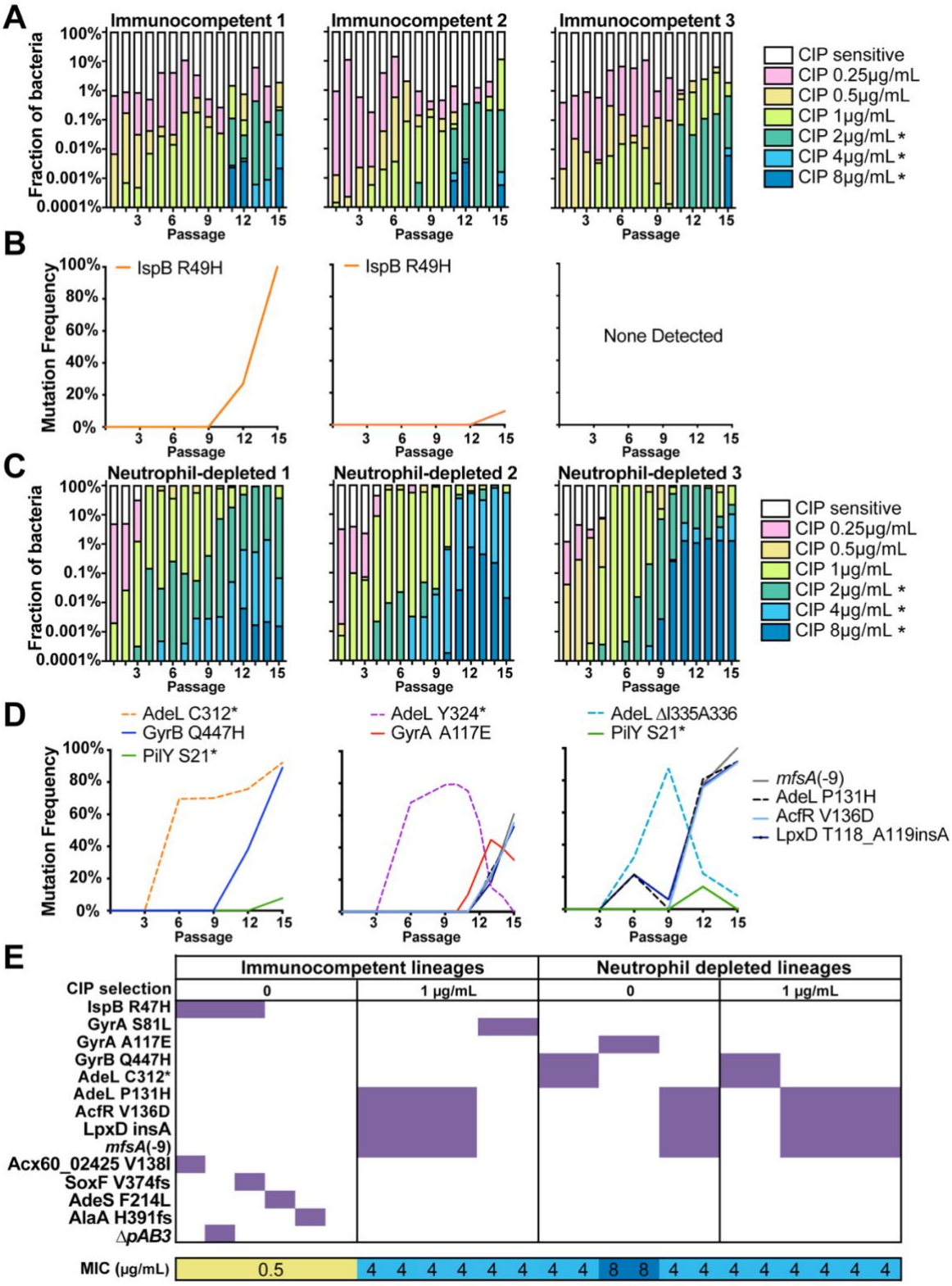

852 **Figure 2. High level ciprofloxacin resistance evolves in a stepwise fashion during passage in**

853 **neutrophil-depleted mice.** (A,C). After each passage, bacteria from lung homogenates were

serially diluted onto LB agar containing noted concentrations of CIP (μg/ml). The fraction of CFU on the graded series of CIP plates was determined for each pool and displayed in stacked bar plots for immunocompetent (A) and neutrophil-depleted (C) mouse infection lineages. The limit of detection was 2.7E-6. (B,D) The gDNA from each bacterial pool was isolated and subject to whole genome sequencing to identify the genomic mutations acquired throughout passaging (after passage 3, 6, 9, 12 and 15). The mutations were detected using a 5% abundance cutoff and filtered against the parent strain AB17978. The relative abundance of each mutation was plotted as a function of passage number from (B) immunocompetent lineages and (D) neutrophil-depleted lineages (D). (E) After 15 passages, the bacterial pool from each lineage was grown on LB with or without CIP (1 μg/mL) to select for single colonies. Colonies were purified and subject to whole genome sequencing and MIC assays. In (E), each column represents a single colony and the rows represent selection criteria, individual mutations and MIC values. The detected mutations with >90% frequency were aggregated for all colonies and the presence of each mutation in a certain colony was highlighted in purple. MICs were labeled and color-coded for all colonies.

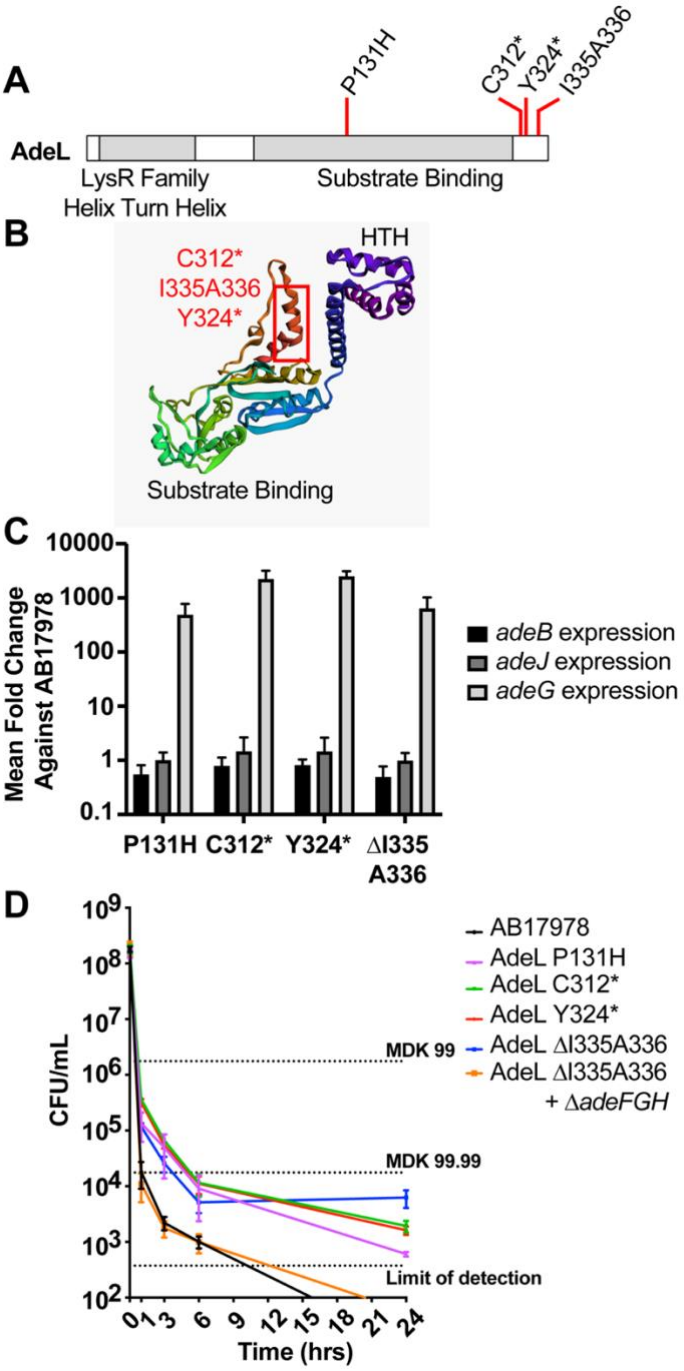

Figure 3. *adeL* mutations drive bacterial persistence through over-expression of the AdeFGH pump. (A). Sites of nonsynonymous changes during *in vivo* passaging and domain structure of AdeL. (B). Locations of nonsynonymous changes on predicted functional domains of AdeL. (C). Mutations in *adeL* selected during mouse passage result in specific overproduction of an AdeL-regulated gene *adeG*. Data were determined by qRT-PCR analysis of pump-encoding

874 components *adeG* (regulated by AdeL) or *adeB* and *adeJ* (components of other pumps) in noted
875 *adeL* mutant backgrounds. (D). Overproduction of AdeL-regulated pump components results in
876 increased persistence in presence of CIP. AB17978 derivatives described in legend were
877 exposed to CIP at 20X MIC for noted times and titered for viability by quantitating CFUs.

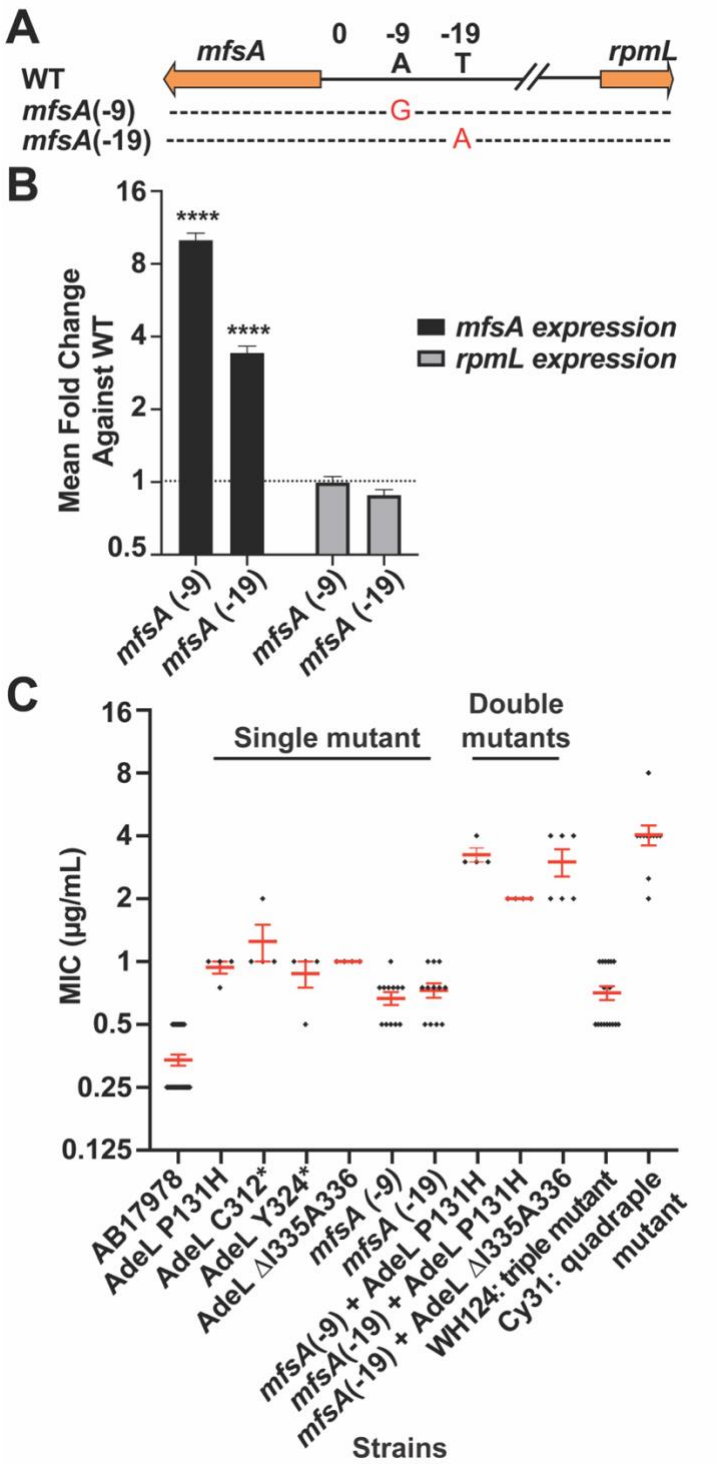

878 **Figure 4. The presence of mutations in *adeL* and *mfsA* is sufficient to explain CIP^{R} in**

879 **strains derived from mouse passage experiments.** A) Two mutations located directly upstream

880 of *mfsA* selected during mouse passaging experiments. B) Transcription levels of *mfsA* and *rpmL*

were determined by qRT-PCR in strains harboring the two mutations upstream of *mfsA*. ****, p < 0.0001. C) Double mutants containing *adeL* and *mfsA* mutations show MICs of CIP that are indistinguishable from evolvedquadruple mutant strain. Data are mean MICs ± SEM.

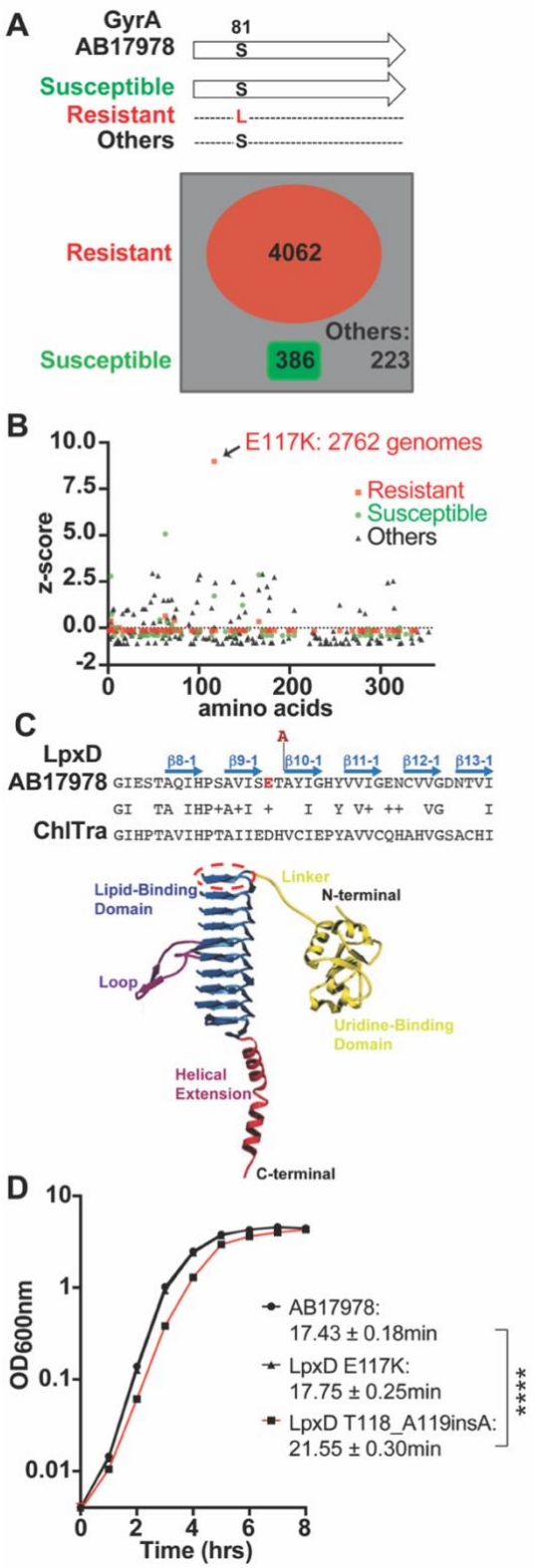

884 **Figure 5. The LpxD E117K allele is tightly linked to clinical fluoroquinolone resistance**.

885 Assembled genomes of 4671 clinical isolates were obtained from PATRIC database[33]. A).

Fraction of genomes having the *gyrA*S81L resistance allele. Among the downloaded genomes, 4062 genomes presented the GyrA S81L allele (shown in red), 386 genomes had the same GyrA allele as ATCC 17978 (shown in green) and the rest had other alleles (shown in black). B) LpxD sequences from all genomes were aligned and compared to ATCC 17978 and the total number of variants per defined amino acid was calculated for each group of genomes. The total number of amino acid changes were normalized and presented as z-scores for each of the three groups, plotted against the residue numbers. C). Structure of *Chlamydia trachomatis* LpxD protein [34] showing the presumed site of the *A. baumannii* E117 based on sequence similarity. D). Broth growth of AB17978 strains differing by single changes in *lpxD*. Shown are strains harboring either the WT, *lpxD* T118A119_insA or *lpxD* E117K alleles.

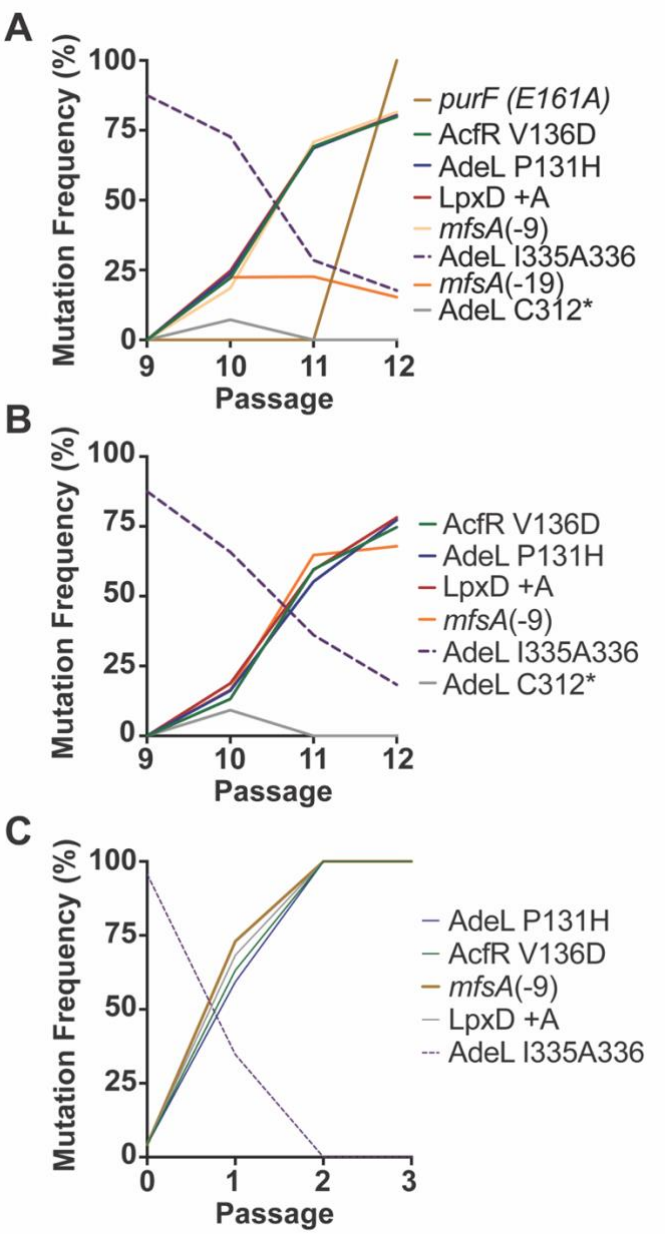

Figure 6. The evolutionary trajectories of isolates acquired throughout passaging in neutrophil-depleted mice is due to fitness advantage in presence of drug. (A,B) A single *adeL* mutant is outcompeted during infection of CIP-treated mice by a quadruple mutant having drug resistant *adeLmfsA* alleles. The passage 9 pool was oropharyngeally inoculated into neutrophil-depleted mice in duplicate and passaged three times, subjecting each passage to deep sequencing. Displayed are relative abundance of all mutations identified in deep sequencing pools of the duplicate (panels A,B) passaging experiments as a function of the passage number.

C) Competition of purfied *adeL* and quadruple mutant having *adeLmfsA* alleles in presence of CIP results in predominance of the quadruple mutant. The two strains were mixed at a ratio 95:5 (single:quadruple mutant), and oropharyngeally inoculated into neutrophil-depleted mice in the presence of CIP through three successive passages. Deep sequencing of the initial inoculum and each subsequent passage was performed to determine the ratio of the two strains, and the relative abundance of each mutation is displayed as a function of passage.

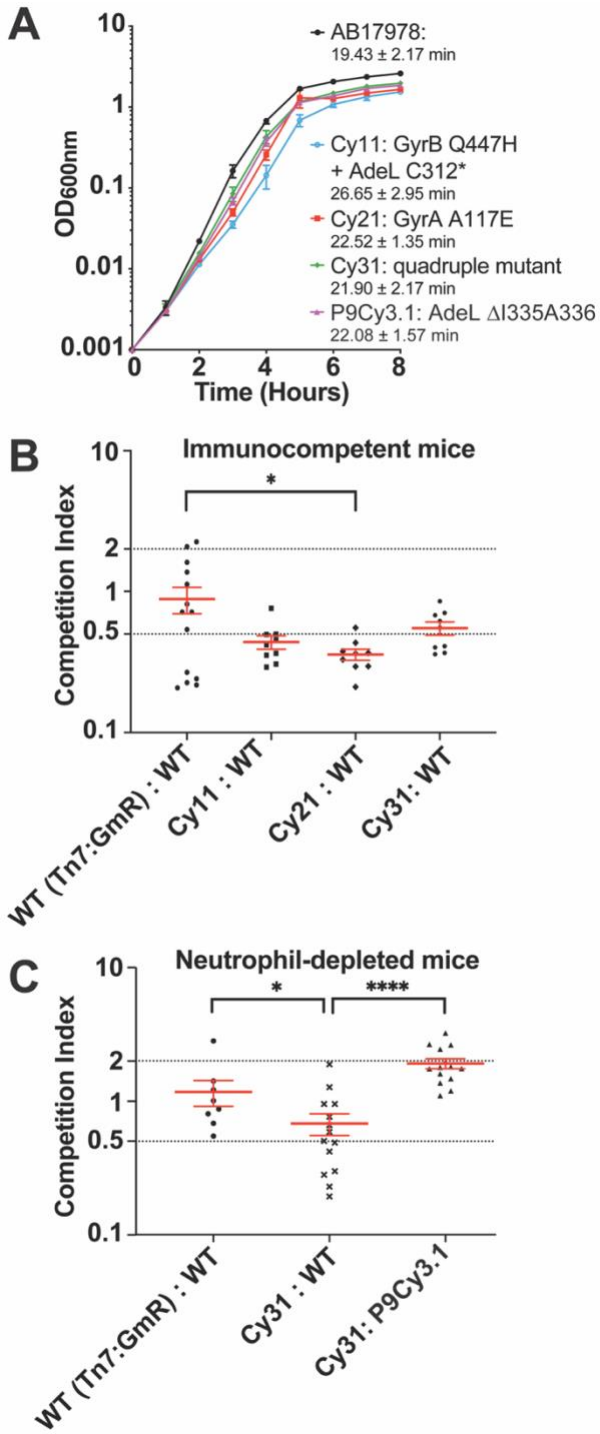

Figure 7. Simultaneous selection for increased resistance and fitness. A) Growth rates in broth culture of noted isolates from passage in mice. B) Neutrophil-replete and C) Neutrophil depleted (cyclophosphamide treated) BALB/C mice were challenged with noted strain combination to determine relative competition index of each pair of strains. C.I. values were

determined by C.I. = (strain1/strain2 output ratio)/(strain1/strain2 input ratio) (Materials and Methods). Data are mean ± SEM, with significance determine by one-way ANOVA followed by Multiple Comparison. *$p<0.05$; ****$p<0.0001$.

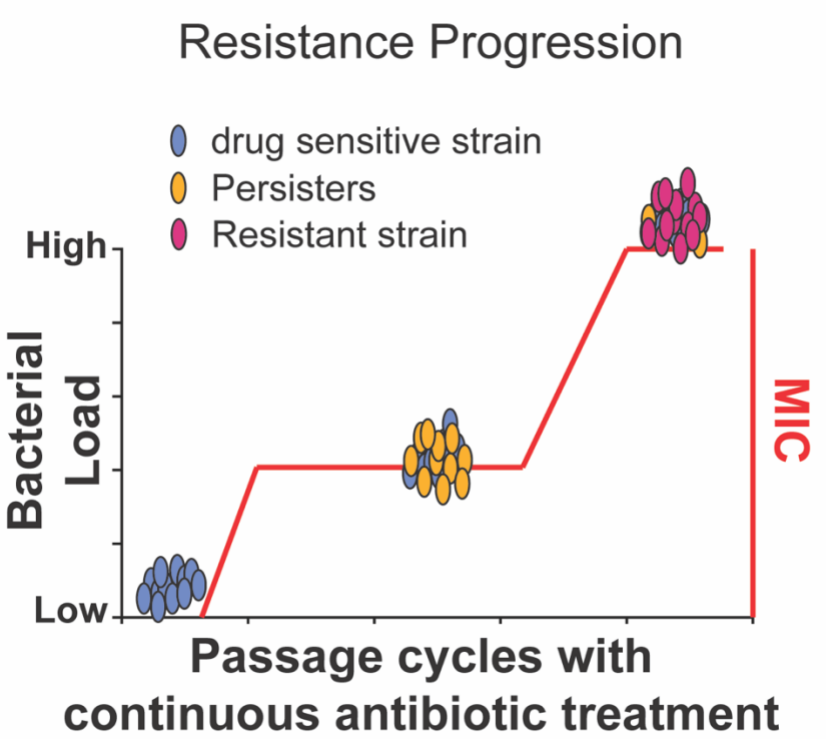

Figure 8. Model of bacterial resistance progression. The antibiotic susceptible inoculum (blue) colonizes poorly in presence of antibiotic. During continued passage with CIP, in the absence of neutrophils, the persister mutants (yellow) arise as first step mutations showing intermediate MICs. With continued passage under the same antibiotic treatment regime, second step mutations arise that have increased fitness in the presence of antibiotic (red) and dominate the population.

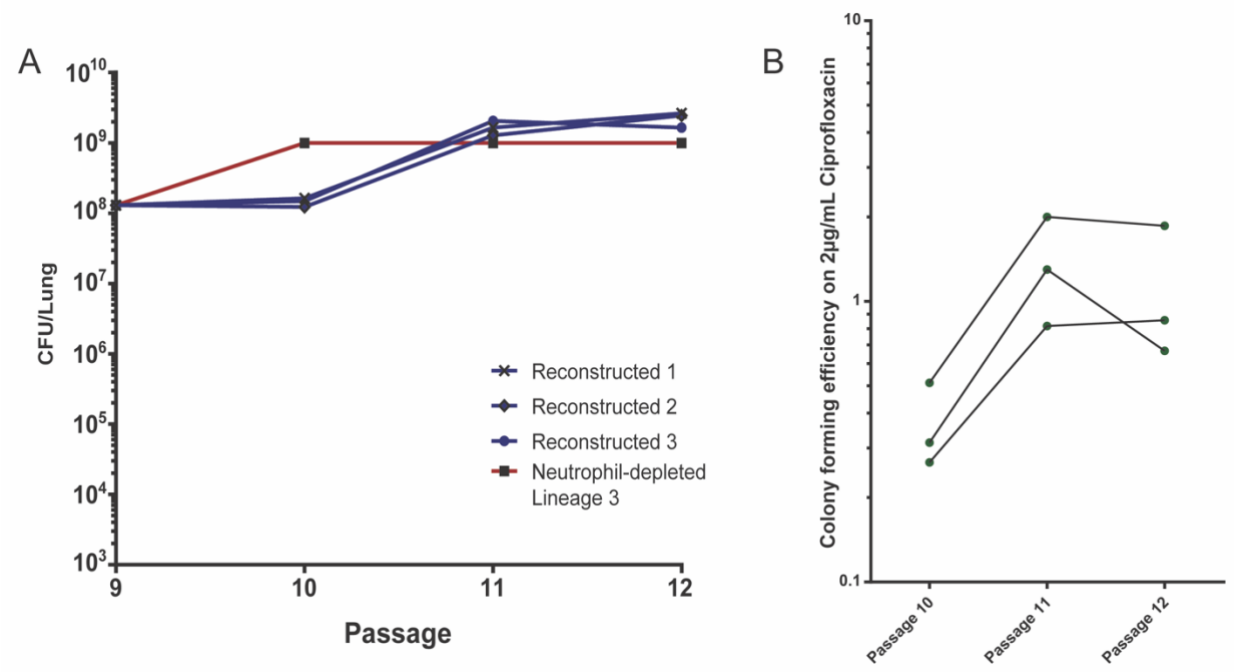

Supplemental Figure 1. Bacterial load and resistance levels to CIP after re-passaging. A) The bacterial load harvested from the lungs after each passage is plotted against the passage number for each lineage. B) CIP resistance level of each pool (after each passage) was assayed via quantification of CFU on LB agar supplemented with CIP.

929 **Table S1. Strains used in this study.**

Clone name	Description	Cipro MIC	reference	Relevant alleles
DH5α	*E. coli:* F⁻ *endA1 glnV44 thi-1 recA1 relA1 gyrA96 deoR nupG purB20* φ80d*lacZ*ΔM15 Δ(*lacZYA-argF*)U169, hsdR17($_{rK^-mK^+}$), λ⁻	N/A	[68]	N/A
DH5α λ*pir*	DH5α encoding π protein	N/A	[69]	N/A
WT/AB17978	*A. baumannii* ATCC 17978	0.5	[70]	N/A
Ab12	Single colonies selected without CIP from immunocompetent L1: 15 passages	0.5	This study	*ispB* R49H; ΔCP012005
Ab11		0.5	This study	*ispB* R49H; *acx60_02425* V138I
Ab21	Single colonies selected without CIP from immunocompetent L2: 15 passages	0.5	This study	*ispB* R49H; soxF V374*fs*
Ab22		0.5	This study	*adeS* F114L
Ab31	Single colonies selected without CIP from immunocompetent L3: 15 passages	0.5	This study	*alaA* H391fs
Ab33		0.5	This study	None detected
CIPAb11	Single colonies CIP 1 μg/mL selection from immunocompetent L1: 15 passages	4	This study	*acfR* V136D; *adeL* P131H; *lpxD* insA; *mfsA*(-9)
CIPAb12		4	This study	*acfR* V136D; *adeL* P131H; *lpxD* insA; *mfsA*(-9)
CIPAb23	Single colonies CIP 1 μg/mL selection from immunocompetent L2: 15 passages	4	This study	*acfR* V136D; *adeL* P131H; *lpxD* insA; *mfsA*(-9)
CIPAb24		8	This study	*acfR* V136D; *adeL* P131H; *lpxD* insA; *mfsA*(-9)
CIPAb32	Single colonies CIP 1 μg/mL selection from immunocompetent L3: 15 passages	8	This study	*gyrA* S81L
CIPAb34		4	This study	*gyrA* S81L
Cy11	Single colonies selected without CIP from neutrophil-depleted mice lineage 1: 15 passages	4	This study	*gyrB* Q447H; *adeL* C312*
Cy12		4	This study	*gyrB* Q447H; *adeL* C312*
Cy21	Single colonies selected without CIP from neutrophil-depleted mice lineage 2: 15 passages	8	This study	*gyrA* A117E
Cy22		8	This study	*gyrA* A117E

Cy31	Single colonies selected without CIP from neutrophil-depleted mice lineage 3: 15 passages	4	This study	*acfR* V136D; *adeL* P131H; *lpxD* insA; *mfsA*(-9)
Cy32		4	This study	*acfR* V136D; *adeL* P131H; *lpxD* insA; *mfsA*(-9)
CIPCy11	Single colonies selected with CIP 1 μg/mL from neutrophil-depleted mice lineage 1: 15 passages	4	This study	*gyrB* Q447H; *adeL* C312*
CIPCy13		4	This study	*gyrB* Q447H; *adeL* C312*
CIPCy21	Single colonies selected with CIP 1 μg/mL from neutrophil-depleted mice lineage 2: 15 passages	8	This study	*acfR* V136D; *adeL* P131H; *lpxD* insA; *mfsA*(-9)
CIPCy22		8	This study	*acfR* V136D; *adeL* P131H; *lpxD* insA; *mfsA*(-9)
CIPCy32	Single colonies selected with CIP 1 μg/mL from neutrophil-depleted mice lineage 3: 15 passages	4	This study	*acfR* V136D; *adeL* P131H; *lpxD* insA; *mfsA*(-9)
CIPCy33		2	This study	*acfR* V136D; *adeL* P131H; *lpxD* insA; *mfsA*(-9)
P9Cy2.1	Single colony selected from neutrophil-depleted mice lineage 2: 9 passages	3	This study	*adeL* Y324*
P9Cy3.1	Single colony selected from neutrophil-depleted mice lineage 3: 9 passages	1	This study	*adeL* ΔI335A336
WH_B3	AB17978 *gyrB* Q447H	0.5	This study	*gyrB* Q447H
WH113	AB17978 *adeL* C312*	1	This study	*adeL* C312*
WH114	AB17978 *lpxD* T118_A119insA	0.25	This study	*lpxD* T118_A119insA
WH309	AB17978 *lpxD* E117K	0.25	This study	*lpxD* E117K
WH115	AB17978 *acfR* V136D	0.25	This study	*acfR* V136D
WH_mfsA_48	AB17978 *mfsA*(-9)	0.75	This study	*mfsA*(-9) A->G
WH_mfsA_12	AB17978 *mfsA*(-19)	0.75	This study	*mfsA*(-19) T->A
WH319	AB17978 *mfs*(-9) *adeL* P131H	4	This study	*mfs*(-9); *adeL* P131H
WH316	AB17978 *mfs*(-19) *adeL* P131H	2	This study	*mfs*(-19); *adeL* P131H

JH1	AB17978 *mfsA*(-19) *adeL* ΔI335A336	3	This study	*mfsA*(-19); *adeL* ΔI335A336
WH124	AB17978 *lpxD* insA *acfR* V136D *adeL* P131H	0.75	This study	*lpxD* insA; *acfR* V136D; *adeL* P131H
EHA8	AB17978 *adeL* ΔIA	1	This study	*adeL* ΔI335A336
EHA15	AB17978 *adeL* P131H	1	This study	*adeL* P131H
EHA123	AB17978 *adeL* ΔIA Δ*adeFGH*	1	This study	*adeL* ΔI335A336; Δ*adeFGH*

930

Table S2. *in vitro* growth rates of LpxD mutants compared to AB17978.

Time (hr)		AB17978				AB17978::LpxD T118_A119insA				AB17978::LpxD E117K			
Optical density at 600nm	0	0.003	0.004	0.005	0.004	0.003	0.004	0.004	0.004	0.004	0.004	0.004	0.004
	1	0.015	0.015	0.015	0.013	0.009	0.011	0.011	0.011	0.014	0.014	0.014	0.013
	2	0.144	0.138	0.143	0.131	0.054	0.059	0.064	0.067	0.124	0.132	0.129	0.12
	3	1.085	1.01	1.01	0.97	0.335	0.37	0.395	0.43	0.935	0.975	0.985	0.825
	4	2.47	2.68	2.445	2.38	1.16	1.27	1.355	1.39	2.36	2.475	2.475	2.27
	5	3.79	3.82	3.78	3.8	2.81	2.98	2.92	3.12	3.64	3.79	3.64	3.76
	6	4.26	4.23	4.3	4.29	3.56	3.52	3.57	3.81	4.41	4.31	4.33	4.12
	7	4.5	4.59	4.67	4.64	3.95	3.97	3.99	4.09	4.69	4.4	4.47	4.55
	8	4.3	4.29	4.58	4.64	4.34	4.36	4.23	4.28	4.44	4.44	4.49	4.32
Doubling time(min)		**17.325**	**17.479**	**17.667**	**17.258**	**21.579**	**21.904**	**21.563**	**21.165**	**17.927**	**17.511**	**17.546**	**18.005**
R^2		**0.999**	**1**	**0.995**	**0.996**	**1**	**1**	**1**	**0.999**	**0.999**	**0.999**	**0.999**	**0.998**

Table S3. ***in vitro*** **growth rates of the isolates acquired from the** ***in vivo*** **passaging experiments.**

Time (hr)		AB17978			AB17978::*adeL* ΔIA			Cy11			Cy21			Cy31		
Optical density at 600nm	0	0.001	0.001	0.001	0.001	0.001	0.001	0.001	0.001	0.001	0.001	0.001	0.001	0.001	0.001	0.001
	1	0.004	0.002	0.004	0.003	0.003	0.003	0.003	0.003	0.003	0.003	0.003	0.003	0.003	0.004	0.003
	2	0.02	0.021	0.025	0.013	0.015	0.014	0.012	0.011	0.011	0.014	0.012	0.013	0.017	0.015	0.015
	3	0.106	0.182	0.201	0.074	0.077	0.055	0.034	0.042	0.03	0.059	0.042	0.049	0.109	0.052	0.094
	4	0.566	0.712	0.747	0.417	0.416	0.284	0.111	0.235	0.084	0.33	0.22	0.222	0.532	0.272	0.488
	5	1.6	1.65	1.8	1.22	1.2	0.99	0.65	0.9	0.51	1.02	0.93	1.95	1.23	1.03	1.24
	6	2.03	2.04	2.12	1.44	1.38	1.3	1.06	1.23	0.94	1.35	1.23	1.22	1.55	1.36	1.55
	7	2.3	2.29	2.5	1.69	1.76	1.63	1.38	1.54	1.1	1.57	1.5	1.39	1.88	1.74	1.78
	8	2.56	2.55	2.7	1.85	1.83	1.89	1.51	1.73	1.37	1.78	1.61	1.57	2.01	1.91	2
Doubling time(min)		**21.463**	**17.147**	**19.693**	**20.828**	**21.57**	**23.843**	**27.629**	**23.331**	**28.985**	**22.828**	**23.691**	**21.038**	**20.606**	**24.404**	**20.682**
R^2		**0.993**	**0.986**	**0.999**	**0.996**	**0.997**	**0.996**	**0.987**	**0.992**	**0.984**	**0.995**	**0.99**	**0.975**	**0.999**	**0.984**	**0.998**